Greywater treatment by anodic oxidation, photoelectro-Fenton and solar photoelectro-Fenton processes: Influence of relevant parameters and toxicity evolution

Paulo Renato dos Santos [1], Maria Eduarda de Oliveira Dourados [2], Ignasi Sirés [4,**], Enric Brillas [4], Rodrigo Pereira Cavalcante [1], Priscila Sabioni Cavalheri [1], Paula Loureiro Paulo [2], Diego Roberto Vieira Guelfi [1], Silvio César de Oliveira [1], Fábio Gozzi [1,3], Amilcar Machulek Junior [1,*]

[1] *Instituto de Química (INQUI), Universidade Federal do Mato Grosso do Sul, Av. Senador Filinto Müller, 1555, MS 79074-460 Campo Grande, Brazil*

[2] *Faculty of Engineering, Architecture and Urbanism and Geography, Federal University of Mato Grosso do Sul, Cidade Universitária, CP 549, Campo Grande, MS, 79070-900, Brazil*

[3] *Campus Floresta, CMULTI, Federal University of Acre, Cruzeiro do Sul, AC 69980-000, Brazil*

[4] *Laboratori d'Electroquímica dels Materials i del Medi Ambient, Departament de Ciència de Materials i Química Física, Secció de Química Física, Facultat de Química, Universitat de Barcelona, Martí i Franquès 1-11, 08028 Barcelona, Spain*

Submitted for publication in the *Process Safety and Environmental Protection*

* Corresponding author: machulekjr@gmail.com (A. Machulek Jr.)

** Corresponding author: i.sires@ub.edu (I. Sirés)

Abstract

In this study, the applicability of factorial design to the treatment of greywater (GW) containing dodecyl-benzene sulfonic acid (LAS) by electrochemical advanced oxidation processes (EAOPs) is demonstrated. At bench scale, anodic oxidation with electrogenerated H_2O_2 (AO-H_2O_2) and photoelectro Fenton (PEF) processes were studied following a 2^3 factorial design with central point insertion, using a first-order mathematical polynomial. In the former process, the combination of a boron-doped diamond (BDD) anode with a carbon-PTFE air-diffusion cathode, both of 3 cm^2, yielded a 76% degradation of LAS at 40 mg L^{-1} along with 52% TOC removal under optimized conditions. The PEF process with 5 mg L^{-1} Fe^{2+} at current density of 77.5 mA cm^{-2} allowed attaining a 63% of LAS degradation and 78% of TOC abatement. The best conditions found for PEF according to the factorial design, in terms of Fe^{2+} concentration and current density, were applied for the treatment of 10 L of raw GW by solar PEF (SPEF) using a compound parabolic collector (CPC) as solar reactor and a filter-press electrochemical cell. A 70% of LAS removal and a 55% of GW mineralization were attained after 240 min of treatment. Artemia salina toxicity tests were performed with effluents resulting from the different methods under optimum conditions, and the SPEF process was proven to be the most effective and promising EAOP for the reduction of GW toxicity.

Keywords: EAOP; Factorial design; LAS degradation; Toxicity; Wastewater treatment.

1. Introduction

Most of the water collected from the natural environment for use in human activities returns carrying some residue that compromises its quality, which puts the environmental balance and public health at risk. It is estimated that around 80% of municipal wastewater is released into the environment without any prior treatment [1]. Greywater (GW) is a common type of urban wastewater that includes all aqueous waste generated in domestic premises (except for toilet flushing), such as kitchen and bathroom sinks, washing machines, dishwashers and bath water. GW accounts for 16-200 liters per capita per day, representing around 75% of the entire volume of sewage generated in a residence [2,3]. The composition and physicochemical characteristics of domestic GW is dependent on multiple factors like the age of the household, eating, hygiene and cultural habits, and purchasing power. In general, domestic GW shows turbidity between 20 and 440 NTU, total coliforms of 6350 to 5.1 10^6 UFC, pH 6-9, total dissolved solids between 520 and 2700 mg L^{-1}, chemical oxygen demand of 60-1340 mg L^{-1}, biochemical oxygen demand of 40-4450 mg L^{-1}), chlorides from 150 to 710 mg L^{-1}, oils and greases from 80 to 330 mg L^{-1}, sodium from 70 to 670 mg L^{-1}, calcium and magnesium between 15 and 60 mg L^{-1} (each), and less than 1 mg L^{-1} for metals such as copper, lead or nickel [3].

Other xenobiotic compounds like endocrine disruptors, solvents, dyes, and surfactants are also found in GW. The anionic surfactants called linear alkylbenzene sulfonates (LAS) stand out as the most ubiquitous among the latter. LAS are very refractory, which makes the treatment of GW by biological methods unfeasible. Their presence induces the appearance of foam in water, seriously destabilizing the treatment units because of the inhibition of the bacterial respiration rates and biodegradation [2,4-6]. LAS are not only toxic, but they are resistant to natural degradation processes such as

hydrolysis and photolysis, making it necessary the use of advanced treatment technologies [7-10].

Recent studies report the presence of LAS in the aquatic natural environment at concentrations from 1.9 to 2406.8 μg L^{-1}, considering both, the dissolved fractions and those adsorbed in sediments [11]. In municipal effluents, LAS have been identified within the concentration range of 2.4-6.7 mg L^{-1}, whereas the anionic surfactants in effluents from the detergent industry the reported values range between 1552 and 1650 mg L^{-1} [12]. These concentrations exceed safety values and pose risks to invertebrate species, fish, algae, and other aquatic plants [4,5,13]. Such difficulties were confirmed by Granatto et al. [14], who evaluated the capacity of a granular sludge biological reactor to remove LAS (0.9 to 11.5 mg L^{-1}) from a municipal effluent in the city of São Carlos (Brazil). A highly variable surfactant removal (30%-90%) was evidenced, demonstrating that the efficiency is dependent on the effluent composition, which in turn varies seasonally. Budikania et al. [15] degraded up to 99% of 100 mg L^{-1} of LAS in 0.02 M NaOH solution by the multi-contact glow discharge electrolysis technique; in that study, H_2O_2 and Fe^{2+} ions as a catalyst were also added, significantly enhancing the LAS degradation indexes. Sakai et al. [16] demonstrated the ability of the UV/H_2O_2 process to degrade 3.5 L of 60 mg L^{-1} LAS solution, using 8 W lamps (λ_{max} = 254 nm) and 100 mg L^{-1} H_2O_2; up to 90% LAS were degraded at 30 min.

Among the most efficient methods for removing persistent organic compounds in aqueous systems, the electrochemical advanced oxidation processes (EAOPs) occupy a preeminent position. These are electrolytic systems that generate large amounts of reactive oxygen species (ROS) capable of degrading organic matter. A widespread type of EAOP is anodic oxidation (AO) [17-20]. The continuous oxidation of organics is ensured by the mass transport of pollutants from the bulk of the solution to the electrode

surface, which in turn is guaranteed by the constant stirring or flowing of the solution during the treatment. The boron-doped diamond (BDD) stands out among the anode materials for AO, owing to its greater robustness and chemical stability. Other materials such as PbO_2, IrO_2 and SnO_2, IrO_2 and their blends are also capable of producing sufficient amounts of $^{\bullet}OH$ on their surface. Furthermore, some of these electrodes are capable of electrogenerating active chlorine species (Cl_2/HClO) in media containing chloride ions. However, they behave as active electrodes that show O_2 evolution at lower overpotentials as compared to BDD; in some cases, they are mechanically or chemically unstable [21,22]. The efficiency of AO can be greatly improved upon coupling with other chemical and photochemical systems.

Another example is the well-established electro-Fenton (EF) process, in which H_2O_2 and Fe^{2+} ion are simultaneously used to produce $^{\bullet}OH$ in the bulk via Fenton's reaction, whose greatest outcome is observed at pH ~3.0 [23-28]. EF process is advantageous over chemical Fenton because the addition of H_2O_2 as synthetic reagent is avoided thanks to its in-situ production at highly efficient carbonaceous materials such as graphite, acetylene black, graphene, carbon nanotubes or carbon fibers [23,28]. Ultraviolet radiation can additionally enhance the performance of the EF process, originating the so-called photoelectro-Fenton process (PEF) [28,29-34]. In recent years, it has been demonstrated that the PEF process becomes even more advantageous and convenient when it is directly fed with solar radiation, which characterizes the solar photoelectro-Fenton (SPEF) process, thereby eliminating the energy demand necessary for UV lamps [28,35,36]. The scheme presented in Fig. 1 summarizes the main reactions that characterize the aforementioned EAOPs.

Insert Fig. 1.

A powerful tool applied to the optimization of technologies like the EAOPs for wastewater treatment is the factorial design coupled to response surface methodology (RSM), since it allows to simultaneously evaluate the synergistic effect of several variables by carrying out a reduced number of experimental tests using computational statistical methods. This is a more efficient and precise methodology as compared to univariate processes because, through RSM analysis, it is possible to obtain predictive equations, based on polynomial models, which describe optimized values of variables as a function of the dependent variables adopted as responses [37-39]. In this context, the 2^k factorial design corresponds to the simplest method of the factorial modality. This is put into practice by performing a number of tests equivalent to 2^k, where k denotes the number of independent variables under investigation [38].

Regarding the GW treatment, several studies have reported the potential improvement of water quality upon the application of different methods. Xu et al [40] showed the possibility of treating GW, collected together with rainwater, by a hydroponics system for the cultivation of *Lonicera Japonica*, achieving removals of 81% COD and 88% of anionic surfactant after 8 d of treatment. Costa et al. [41] described the ability of *Penicillium chrysogenum* to biodegrade a synthetic effluent that mimicked GW containing LAS, obtaining 99.5% removal of 12 mg L^{-1} of the surfactant after 5 incubation days. Bakheet et al [42] applied a combined biofiltration system with *Carex apressa* plant culture vessels and electrochemical disinfection using a boron-doped diamond (BDD) anode (40 cm^2) in a reflux system with a capacity of 1 m^2 d^{-1}. Removals of up to 90.4% TOC, 88.9% *E. coli* and 88.3% total coliforms were found, with an estimated energy consumption of 0.63–0.83 kWh m^{-3}. Anaerobic filters followed by UV photolysis was employed by Couto's group [43] to reduce 73% BOD_5, 72% COD, 77% TSS, 88% turbidity and 60% NO_3^-, being estimated a consumption of 64 kWh m^{-3} for total

disinfection. Kim and Park [44] used ultrafiltration to remove 65% of 1000 mg L^{-1} sodium dodecyl-benzene sulfonate using 1 kDa ceramic membrane by applying 1.5 bar at room temperature. Oh et al. [45] demonstrated the possibility of applying ozonation as post-treatment of filtration steps, estimating an energy consumption of 1.80 kWh m^{-3} for total disinfection of the GW. Chemical coagulation–flocculation combined with UV photolysis was applied by Terechova et al. [46] to remove LAS from a synthetic effluent. Under optimum conditions, between 71.3% and 74.6% LAS were removed from laundry wastewater. A recent study by Patel et al. [47] pointed out the feasibility of treatment of GW by electrocoagulation process using Al electrodes, reaching 70% COD removal after 60 min. In that work, the authors applied statistical methodologies to optimize the treatment and estimated a consumption equal to 0.153 kWh m^{-3}. Mostafazadeh et al. [48] proposed a combined process using membrane filtration, electrochemical technologies, and adsorption for treating laundry wastewater containing nonylphenol ethoxylates (NPEO3-17). A 50% COD and 75% of NPEO3-17 removal was obtained. Ghambari and Martínez-Huitle [49] showed the viability of EF and PEF, in the presence and absence of peroxymonosulfate, for washing machine effluent treatment; 99.5% COD and 97% TOC were eliminated under optimum conditions. Thirugnanasambandham and Sivakumar [50] also presented a study on the treatment of GW using EF-type methods. In their study. a statistical methodologies of factorial design and response surface analysis was used to assess the influence of parameters and, under the best conditions, 99% COD removal was obtained. Table 1 summarizes the main data reported in this series of papers above, as compared to results obtained in the present work that will be discussed below.

Insert Table 1

This paper aims to study the feasibility and efficiency of the AO with in-situ H_2O_2 electrogeneration (AO-H_2O_2), PEF and SPEF processes for the treatment of raw GW

144 containing LAS using a factorial design. In AO-H_2O_2, the synergism between the
145 independent variables (LAS concentration, current density (*j*) and time (*t*)) for LAS
146 degradation and solution mineralization was studied. In PEF, a similar study was carried
147 out, but including the initial Fe^{2+} concentration as variable of interest. The best values of
148 current intensity and initial Fe^{2+} concentration found from the factorial design for PEF
149 were further applied to the SPEF treatment of GW using a compound parabolic collector
150 (CPC) as solar photoreactor. In all cases, acute toxicity tests with Artemia salina were
151 made under optimized treatment conditions. To the authors' knowledge, this is the first
152 GW treatment study focused on AO-H_2O_2 and PEF processes that includes factorial
153 design for monitoring LAS degradation and TOC removal. Furthermore, the best
154 conditions found were further used to assess the toxicity evolution in SPEF process.

155 **2. Materials and methods**

156 *2.1 Actual greywater*

157 During two weeks, two samples of raw clear greywater (10 L each) were obtained
158 from a pilot system for generating domestic effluents installed at the Environmental
159 Engineering Laboratory of the Center for Exact and Earth Sciences (CCET of the Federal
160 University of Mato Grosso do Sul, in Campo Grande campus). The system is equipped
161 with a kitchen sink, a bathroom sink, a bath shower, and a washing machine, used
162 voluntarily by resident academics, with an average GW generation in the order of 0.5 m^3
163 d^{-1}. The physicochemical characteristics of the GW produced at pilot unit, which are
164 summarized in Table 2, are similar to those reported in the literature for this type of
165 effluent. Up to 20 L of sample were collected weekly and immediately stored at 4 ºC in
166 sterile, tightly capped opaque flasks.

167 **Insert Table 2**

2.2 Reagents

Linear dodecylbenzene sulfonic acid (LAS, CAS No. 68584-22-5, 70%, $C_{18}H_{30}O_3S$), sodium sulfate (CAS No. 7757-82-6, ≥99.0%), heptahydrate ferrous sulfate (CAS No: 7439-89-6, 97%) and catalase (CAS No. 9001-05-2, 10,000-50,000 units (mg protein)$^{-1}$) were acquired from Sigma-Aldrich. Ultrapure water (conductivity < 0.05 μS cm^{-1} at 25 °C) was supplied by a Millipore Milli-Q system. Other reagents and solvents of analytical grades were supplied by Vetec Quimica Fina or Sigma-Aldrich.

2.3 Bench-scale degradation system

Solutions of 100 mL of GW spiked with LAS and 0.050 M Na_2SO_4 as supporting electrolyte were treated in a benchtop electrochemical reactor with a capacity of 150 mL. This reactor was undivided and jacketed for water recirculation at 25 ºC. To operate under AO-H_2O_2 conditions, a BDD thin film (B doping of 700-800 ppm) electrode supported on a *p*-type monocrystalline Si wafer (NeoCoat®, Switzerland) was used as the anode, whereas a carbon-PTFE air-diffusion cathode (E-TEK, USA) served to electrogenerate H_2O_2 at constant air flowrate of 2 L min^{-1}. Both electrodes had a geometric area of 3 cm^2 and the gap between them was 1 cm. In order to carry out the PEF treatment, the BDD anode was replaced by a platinum foil of 3 cm^2 (SEMPSA, Spain, ≥99%), and the solution surface was irradiated with a Philips TL 4 W BLB UVA fluorescent lamp (λ_{max} = 360 nm, P_0 = 2.92 10^{19} photons s^{-1}) placed 6 cm above the waterline [28,31]. In all experiments, a constant stirring was kept by a magnetic bar at 700-800 rpm. DC current was supplied from an FA 3003-DC Instrutherm source, whereas the cell voltage was monitored with an ET-1507B (Minipa) digital multimeter. To ensure cleanliness and activation of electrode surfaces, before of each degradation experiment, electrolysis was conducted in 0.1 M H_2SO_4 at j = 100 mA cm^{-2} for 30 min. Fig. 2a schematizes the most notable elements of the bench-scale degradation system used.

193 **Insert Fig. 2**

194 *2.4 Analytical methodologies*

195 The physicochemical characterization of GW was performed at the UFMS
196 Environmental Quality Laboratory, including as parameters: chemical oxygen demand
197 (COD), biochemical oxygen demand at 5 d (BOD_5), chloride (Cl^-), ammonia (NH_3, 4500-
198 NH_3 B/C method), nitrate (NO_3^-, 4110 B/C), phosphate (PO_4^{3-}, 4500-P B/E) and total and
199 dissolved solids quantified in accordance with SMWW [51]. The total nitrogen was
200 quantified by catalytic oxidation via chemiluminescence (Shimadzu TOC-CSN coupled
201 to TNM-1 module). In the PEF and SPEF trials, the initial pH was adjusted to 3.0 using
202 solutions of 50% (v/v) H_2SO_4 or NaOH and measuring its value on a Crison 2000 pH
203 meter, which also served for monitoring it during the experiments. The AO-H_2O_2 trials
204 were carried out at the natural pH of the effluent (6.7-7.6). Al, Ba, Ca, Zn, Mn, Ni, Hg,
205 Cr, Cd, and Pb were quantified with a 3111-B direct air-acetylene flame atomic
206 absorption method. The turbidity was measured using an Orion AquaFast turbidimeter
207 (Thermo Scientific), and the conductivity with a Sension5 conductivity meter (Hach).
208 LAS concentration was determined from previously diluted samples by Methylene Blue
209 absorption spectroscopy, according to Jurado et al. [52]. 5 mL of LAS standard solution
210 or previously diluted samples were added to 4 mL of dichloromethane, 100 µL of 50 mM
211 sodium tetraborate buffer solution at pH 10.5, and 100 µL of slightly acidic 1 g L^{-1}
212 Methylene Blue solution. The mixture was stirred for 1 min, followed by phase separation
213 and then, the absorbance of the organic phase was measured using a U-3900
214 spectrophotometer (Hitachi) set at λ = 652 nm. To eliminate the influence of sample
215 composition-related factors, the calibration curve was prepared using GW of each
216 sampling as the solvent. The range was 0 – 2.5 mg L^{-1} LAS, yielding LOQ = 0.95 – 0.73

mg L^{-1} and LOD = 0.37 – 0.22 mg L^{-1}. The experimental degradation percentage was calculated according to Eq. (1):

$$Y_{\%\mathrm{Deg}} = \frac{([\mathrm{LAS}]_\mathrm{i} - [\mathrm{LAS}]_\mathrm{f})}{[\mathrm{LAS}]_\mathrm{i}} \times 100 \qquad (1)$$

where $[LAS]_i$ and $[LAS]_f$ correspond to the initial and final concentration of the surfactant during the application of EAOPs.

The mineralization was followed by the decay of total organic carbon (TOC) content, determined by the catalytic oxidation method using a VCPN analyzer (Shimadzu) duly calibrated with potassium phthalate and $NaHCO_3$, presenting LOQ = 0.180 mg L^{-1} and LOD = 0.053 mg L^{-1}. The data from this analysis allowed calculating the percentage of experimental mineralization taken as a response to the factorial plan according to Eq. (2):

$$Y_{\%\mathrm{Min}} = \frac{(\mathrm{TOC}_\mathrm{i} - \mathrm{TOC}_\mathrm{f})}{\mathrm{TOC}_\mathrm{i}} \times 100 \qquad (2)$$

where TOC_i and TOC_f are the total initial and final dissolved organic carbon of the GW obtained during the application of the EAOPs, respectively.

The energy consumption per unit mass of total dissolved organic carbon (EC_{TOC}) was estimated according to Eq. (3) [23]:

$$\mathrm{EC}_\mathrm{TOC} = \frac{E_\mathrm{cell} I\, t}{V_\mathrm{s}(\Delta\mathrm{TOC})_\mathrm{exp}} \qquad (3)$$

where E_{cell} corresponds to the electric potential difference arising in the electrochemical cell (V), I is the electric current (A), t is the time (h), V_s is the volume of treated solution (L), and $(\Delta TOC)_{exp}$ is the TOC decay at the end of the experiment (mg L^{-1}).

2.5 Factorial design

The synergism between variables of interest in the different EAOPs applied for GW treatment at bench scale was studied from a 2^3 factorial design, with triplicates at the central point. Statistica 14 software (TIBCO Software Inc.) trial version was employed for the computational statistical analysis. In AO-H_2O_2, current density (X_j), time (X_t) and

LAS concentration ($X_{[LAS]}$) were listed as independent variables. The interactions of up to three independent variables (3-way interactions), resolution R = FULL, consideration of curvature check, 2**(K-p) standard designs (Box, Hunter & Hunter) mode were the software conditions chosen because they yielded the minimal residuals of prediction model. In PEF trials, the LAS concentration was fixed at 40 mg L^{-1} and current density (X_j), time (X_t) and initial Fe(II) concentration ($X_{[Fe^{2+}]}$) were listed as independent variables, and the interactions of up to two independent variables (2-way interactions), with curvature check, in 2-level screening (Placket-Buman) design mode were the selected software conditions. The values considered for the independent variables in all assays of both EAOPs are presented in Table S1. In AO-H_2O_2 and PEF, the degradation of LAS ($Y_{\%Deg}$) and the mineralization of the organic load ($Y_{\%Min}$) contained in GW were considered as dependent variables (i.e., response). The interaction between the independent variables of factorial design was obtained from a second-order polynomial, as follows:

$$Y = \beta_o + \sum_{i=1}^{k} \beta_i X_i + \sum_{1 \le i \le n}^{k} \beta_{in} X_i X_n \qquad (4)$$

where k denotes the number of independent variables (k = 3), Y represents the response of the dependent variable ($Y_{\%Deg}$, $Y_{\%Min}$), β_o is a constant, β_i and β_{in} account for the linear effects related to the linear X_i, the X_iX_n interaction term, respectively [53].

2.6 Pilot unit for SPEF treatment

Using the best conditions of PEF, the SPEF treatment of 10 L of GW containing 40 mg L^{-1} LAS was performed in a pre-pilot unit equipped with a press-filter electrochemical cell coupled to a CPC solar photoreactor. The recirculation system included a 20 L reservoir tank provided with mechanical stirring. This reservoir was connected through a PVP pipe (3/4") to a centrifugal liquid pump (Dancor, CP-4R, ¼ hp M) that operated at a

constant flowrate of 180 L min^{-1}, as determined by means of a flowmeter. This flowrate was selected based on the results of Alcaide et al. [54], who used a similar flow system. The electrochemical press-filter cell was arranged as described in [28], and equipped with a pair of electrodes like those employed in the bench-scale PEF, but their exposed area was 20 cm^2 and the interelectrode gap was 1.2 cm. The CPC module consisted of five borosilicate glass tubes (internal diameter 28 mm, length 851 mm and thickness 4 mm, with total illuminated area of 0.2248 m^2) connected in series by polypropylene joints, placed above anodized aluminum mirrors supported on an aluminum frame, tilted 15° and facing to East. The experiments were carried out at the Chemistry Institute of the Federal University of Mato Grosso do Sul, Campo Grande city, Brazil (20°30'20.6"S 54°37'02.1"W), in cloudless days. Solar global radiation was measured in situ using a 1 cm^2 solar calibration cell attached to a PCLAB voltmeter (V&A Instruments) matching 100 mV to 100 mW m^{-2}, positioned at the same angle of the CPC module. Fig. 2b presents a scheme with the principal elements of the pilot unit for the SPEF treatment.

2.7 Acute toxicity

The acute toxicity tests with Artemia salina as indicator organism were carried out in triplicate according to Da Silva et al. [39]. The newly hatched larvae of this microcrustacean obtained in synthetic seawater at 30 g L^{-1} and pH 8–9 were subjected to aeration for 48 h at 25 ºC, with a 16 h light photoperiod in a static system containing the effluents obtained from the optimized treatments. Catalase was always added for H_2O_2 removal. The dead brine shrimp larvae were counted as recommended in the literature (ten individuals per well) [55], and then compared with controls of untreated GW. Finally, the LC_{50} values (lethal concentration that causes a mortality of 50% of the test organism) were used in the Spearman-Karber probability model using the Minitab version 19 software.

3. Results and discussion

3.1 Factorial design for AO-H_2O_2 process

The observed responses of the factorial design (LAS degradation – $Y_{\%Deg}$, solution mineralization – $Y_{\%Min}$), obtained either experimentally or from the prediction model (considering a 95% confidence limit and alpha value of 0.05 for the results in all experiments), are presented in Table 3, where the results of energy consumption per unit of TOC are also presented for all degradation experiments being in the range of 0.13 - 23.92 kWh (kg TOC)$^{-1}$. These results are illustrated in Fig. 3, in which the fitted correlations between the theoretical model and the experimental results are shown using a linear regression. For both, the LAS degradation response (Fig. 3a) and solution mineralization (Fig. 3b), a low error (MS residual), and a good linear fitting with optimal regression coefficients for $Y_{\%Deg}$ (R^2 =99.978% and R^2_{adj} = 99.890%) and $Y_{\%Min}$ (R^2 = 99.975% and R^2_{adj} = 99.875%) can be observed. The R^2_{adj} coefficient value greater than 95% suggests that less than 5% of the total variations cannot be explained by the mathematical model obtained [50].

Insert Table 2

Insert Fig. 3

The application of statistical models such as factorial design to be studied by analysis of variance (ANOVA) is an important tool that allows identifying the influence of each independent variable studied and their interactions. Table 4 presents the ANOVA results of the linear and or quadratic regression model obtained for $Y_{\%Deg}$ and $Y_{\%Min}$ responses of factorial design in AO-H_2O_2. The sum of squares (SS) measures the influence of the corresponding variable on the variation of the response values obtained in the factorial design table, the degrees of freedom (df) correspond to the number of columns of responses obtained, and the mean of the squares (MS) is related to the ratio between SS

and df. The F-value corresponds to the ratio between MS and MS residual (error) generated from the prediction model (here 0.9331 for $Y_{\%Deg}$, and 0.2973 for $Y_{Min\%}$), whereas p-value is obtained as a statistical function of F-value considering the degrees of freedom of the MS values and the error value (MS residual). High F-values and low p-values (lower than 0.05) evidence that the statistical model is significant with a probability level of 95%. A p-value lower than 0.05 can be interpreted as having less than a 5% probability of the null hypothesis of influence of the variable, or synergism between the variables in the degradation and mineralization responses being true [56].

Insert Table 4

In accordance with the ANOVA results, Table 5 presents the effect of the variables and their correlations in the statistical models that describe the response variables of the treatment of GW. The greater the effect modulus, the more significant the influence of the variable on the response. The t-value corresponds to the normalized estimated effect, which consists of the ratio of the effect and its corresponding standard error (shown as Standardized Effect Estimate (Absolute Value) in the Pareto charts in Fig. 4), and the p-value is a cumulative distribution function of the statistical test distribution over the null hypothesis, note that the p-values for ANOVA results (Table 4) and the p-values obtained for the estimated coefficients are reciprocal.

Insert Table 5

The time variable (X_t) had the greatest effect on GW treatment, as can be confirmed in Fig. 4, in which the Pareto charts denote the influence of the independent variables and their interactions on $Y_{\%Deg}$ (Fig. 4a) and on $Y_{\%Min}$ (Fig. 4b) responses. In this case it is considered influential, as reported in other studies that assume the reaction time as an independent variable of a statistical factor model [50,53,56]. Reciprocal to the results shown in Tables 4 and 5, the estimated effects for the isolated variables $X_{[LAS]}$ (1), Xj (2)

or X_t (3) give the contributions to the linear regression model. The effects described by (1 by 2), (1 by 3), (2 by 3) and (1*2*3) correspond to the contributions to the quadratic regression model and interaction of up to 3 variables, respectively. Regarding the LAS degradation (Fig. 4a), a relevant synergistic effect between the variables LAS concentration and current density (i.e., $X_{[LAS]}$ and X_j) can be noticed, as also found between the three variables simultaneously. For GW mineralization (Fig. 4b), synergistic effects were observed between LAS concentration and time (i.e., $X_{[LAS]}$ and X_t).

Insert Fig. 4

All variables evaluated, except current density, had a positive effect on the responses ($Y_{\%Deg}$ and $Y_{\%Min}$). This can be confirmed in Fig. 5a and 5b, respectively, where the graphs of individual and composite desirability of the variable on the responses are highlighted. This was estimated under optimized conditions, which are related to a desirability (D) equal to zero for the smallest response value, and D equal to 1 for the high response value (optimal desirable condition). The negative effect of the current density variable on the $Y_{\%Min}$ response can be justified by the gradually larger extent to which some side faradaic reactions ("side" meaning less productive reactions as compared to reaction (1) that yields the very powerful hydroxyl radical) occur on the surface of the BDD anode. These include the oxygen evolution from reaction (5), ozone electrogeneration from reaction (6) and the formation of the $S_2O_8^{2-}$ ion from reaction (7), thereby inhibiting the formation of $^{\bullet}OH$ by reaction, Fig. 1. Also, the accumulation of an excess of H_2O_2 at the air-diffusion cathode can be detrimental, since it then reacts on the surface of the anode, either directly or through $^{\bullet}OH$, yielding the weaker hydroperoxyl radical ($HO_2^{\bullet}$) via reactions (8) and (9). Overall, the promotion of reactions (5)-(9) reduces the oxidation rate of the organic matter present in the GW [49].

$$2BDD(\ ^{\bullet}OH) \rightarrow 2BDD + O_2 + 2H^+ + 2e^- \qquad (5)$$

$$3H_2O \rightarrow O_3 + 6H^+ + 6e^- \quad (6)$$

$$2SO_4^{2-} \rightarrow S_2O_8^{2-} + 2e^- \quad (7)$$

$$H_2O_2 + {}^{\bullet}OH \rightarrow H_2O + HO_2^{\bullet} \quad (8)$$

$$H_2O_2 \rightarrow HO_2^{\bullet} + H^+ + e^- \quad (9)$$

Insert Fig. 5

The use of BDD as anode material in combination with the presence of active inorganic ions in the effluent led to the occurrence of other parasitic reactions on the anode surface, especially as the applied current was increased. For example, the direct oxidation of CO_3^{2-} may result in radicals (via reaction (10)) and percarbonate (via reactions (11) or (12)). Similarly, the indirect oxidation of CO_3^{2-} or HCO_3^- by hydroxyl radicals adsorbed on the surface of the BDD anode (i.e., BDD($^{\bullet}OH)_{ads}$) according to reactions (13) and (14), respectively, is feasible. Moreover, chlorine oxidants are generated upon chloride oxidation from reactions (15)-(17), whereas $S_2O_8^{2-}$ and $SO_4^{\bullet-}$ can be electrogenerated from SO_4^{2-} oxidation via reactions (7), (18) and (19) [57]:

$$CO_3^{2-} \rightarrow CO_3^{\bullet-} + e^- \quad (10)$$

$$2\,CO_3^{2-} \rightarrow C_2O_6^{2-} + 2\,e^- \quad (11)$$

$$2CO_3^{\bullet-} \rightarrow C_2O_6^{2-} \quad (12)$$

$$BDD({}^{\bullet}OH)_{ads} + CO_3^{2-} \rightarrow BDD + CO_3^{\bullet-} + OH^- \quad (13)$$

$$2BDD({}^{\bullet}OH)_{ads} + 2\,HCO_3^- \rightarrow 2BDD + C_2O_6^{2-} + H_2O \quad (14)$$

$$Cl_2 + H_2O \rightarrow HOCl + H^+ + Cl^- \quad (15)$$

$$HOCl \leftrightarrows ClO^- + H^+ \quad (16)$$

$$ClO_2^- \rightarrow ClO_2^{\bullet} + e^- \quad (17)$$

$$SO_4^{2-} + {}^{\bullet}OH \rightarrow SO_4^{\bullet-} + 2\,H_2O \quad (18)$$

$$2\,SO_4^{\bullet-} \rightarrow S_2O_8^{2-} \quad (19)$$

Regarding the synergism between independent variables observed in the AO-H_2O_2 GW treatment, both for $Y_{\%Deg}$ (i.e., $X_{[LAS]}$ and X_j) and $Y_{\%Min}$ (i.e., $X_{[LAS]}$ and X_t), the RSM results are depicted in Fig. 6a and 6b, respectively. For $Y_{\%Deg}$ (Fig. 6a), the response surface was calculated at X_t = 65 min, revealing that the best LAS degradation response is obtained at the highest values of the correlated variables. In the case of $Y_{\%Min}$ (Fig. 6b), the response surface was calculated at X_j = 55 mA cm^{-2}, also demonstrating that the best responses were found as the correlated variables increased their values with a maximal for 80 mg L^{-1} LAS.

Insert Fig. 6

The fitting function of regression prediction model obtained by RSM shown in Fig.4a ($Y_{\%Deg}$) and 4b ($Y_{\%Min}$) is given by Eq. (20) and Eq. (21), respectively. The signs of the estimated regression coefficients account for the effect of the factors on the process, with the positive ones being related to a greater degradation/mineralization upon increase of the given value of the variable within the tested range. Note that the variables $X_{[LAS]}$ and X_j present a synergistic effect for $Y_{\%Deg}$, whereas for $Y_{\%Min}$ a synergistic effect appears between $X_{[LAS]}$ and X_t [39].

$$Y_{\%\mathrm{Deg}} = 9.9644 - 0.19665\,X_{[LAS]} - 0.3355\,X_j + 0.0076\,1\,X_{[LAS]}\,X_j - 0.00307 \times 65\,X_{[LAS]} - 0.00220 \times 65\,X_j + 0.00003 \times 65\,X_{[LAS]}\,X_j + 50.415 \quad (20)$$

$$Y_{\%\mathrm{Min}} = 15.755 + 0.01638\,X_{[\mathrm{LAS}]} - 0.16754\,X_t + 0.00006 \times 55\,X_{[\mathrm{LAS}]} + 0.00692\,X_{[LAS]}\,X_t + 0.00457 \times 55\,X_t - 0.00007 \times 55\,X_{[\mathrm{LAS}]}\,X_t - 12.937 \quad (21)$$

Other interactions of the independent variables in the $Y_{\%Deg}$, and $Y_{\%Min}$ responses can be observed in Fig. S1a and S1b, respectively, where they are presented as desirability 2D-surface graphs. Here it is possible to confirm the positive effect of the variable X_t

when correlated with the other variables for the $Y_{\%Deg}$ and $Y_{\%Min}$ responses. In contrast, the antagonistic behavior of the variable X_j in the response $Y_{\%Min}$ can be observed, with the highest response values at the lowest values of this variable.

3.3 Factorial design for PEF process

The results of $Y_{\%Deg}$ and $Y_{\%Min}$ responses obtained from the factorial design developed for the PEF process applied to the GW treatment, now considering the initial concentration of Fe^{2+} catalyst (i.e., $X_{[Fe^{2+}]}$), current density (i.e., X_j) and treatment time (X_t) as the independent variables, are summarized in Table 6, where the results of energy consumption per unit of TOC are also presented for all degradation experiments with values in the range of 0.05 – 6.52 kWh $(kg\ TOC)^{-1}$. With 95% confidence limit obtained for the 11 experiments. Fig. 7a and 7b depict the very good linear regression coefficients for both $Y_{\%Deg}$ (R^2 = 99.337% and R^2_{adj} = 97.790%) and $Y_{\%Min}$ (R^2 = 98.708%; R^2_{adj} = 96.771%), respectively, revealing a great robustness of the polynomial model, as well as a low experimental error (MS residual equal 8.5987 for $Y_{\%Deg}$ and 14.930 for $Y_{\%Min}$).

Insert Table 6

Insert Fig. 7

The ANOVA results for PEF treatment are depicted on Table 7, revealing a significant effect of the variable X_t and the interaction between $X_{[Fe2+]}$ and X_j on the $Y_{\%Deg}$ response. The same is observed for the $Y_{\%Min}$ response plus the contribution of $X_{[Fe2+]}$ and Xj alone. Table 8 presents the corresponding estimated effects of the independent variables obtained from the regression model. Isolated or in interaction, antagonistic behavior is observed for the variables $X_{[Fe2+]}$ and X_j for the treatment of GW by PEF, as confirmed by the negative signs of the coefficients.

Insert Table 7

Insert Table 8

The increase in X_j value results in parasitic reactions, as described in section 3.1 for AO-H_2O_2 by reaction (8). On the other hand, the high amount of Fe^{2+} in Fenton reaction systems can reduce the amount of $^{\bullet}OH$ available in the bulk solution according to reaction (22):

$$Fe^{2+} + {}^{\bullet}OH \rightarrow Fe^{3+} + OH^{-} \qquad (22)$$

In Fig. 8, the Pareto charts allow quantifying the effect of the variables on the $Y_{\%Deg}$ and $Y_{\%Min}$ responses. Similarly, to the AO-H_2O_2 treatment, the X_t showed the greatest effect on both $Y_{\%Deg}$ and $Y_{\%Min}$ in the PEF treatment of GW. For $Y_{\%Deg}$ (Fig. 8a), the synergistic effect is observed for $X_{[Fe^{2+}]}$ and X_j. In contrast, for $Y_{\%Min}$ (Fig. 8b), all independent variables were significant, with synergism between $X_{[Fe^{2+}]}$ and X_j greater than that observed for $Y_{\%Deg}$. This is confirmed in Fig. 9, where the excellent levels of responses obtained upon variation of intensity of the independent variables are demonstrated. In the case of $Y_{\%Deg}$ (Fig. 9a) and $Y_{\%Min}$ (Fig. 9b), only X_t presented a positive effect on the responses, whereas the most pronounced negative effect of the variables X_j and $X_{[Fe^{2+}]}$ are found for $Y_{\%Min}$.

Insert Fig. 8

Insert Fig. 9

The response surfaces for the most significant interactions between the factorial design variables of the PEF process in the treatment of GW, considering X_t = 65 min, are shown in Fig. 10. At an electrolysis time of 120 min, using [Fe^{2+}] = 5 mg L^{-1} and current density j = 77.5 mA cm^{-2}, the best responses for degradation (63%, Table 6) and mineralization (78%, Table 6) were obtained. Ambiguously, the response surface of Fig. 10a suggests that a decrease in X_j would lead to higher LAS degradation rate, considering the optimum concentration range is between 14-22 mg L^{-1} for the variable $X_{[Fe^{2+}]}$.

A distinct response surface is observed for $Y_{\%min}$ in Fig. 10b, since the best indices of GW mineralization are obtained at the highest values of X_j and lowest values of $X_{[Fe^{2+}]}$. These best results obtained at low current density are consistent with those reported by other authors in similar treatment systems [29].

Insert Fig. 10

Finally, the polynomial mathematical model for predicting the response surfaces based on the independent variables of the factorial planning developed for PEF treatment are given by Eq. (23) and (24) for the responses $Y_{\%Deg}$ and $Y_{\%Min,}$ respectively.

$$Y_{\%\mathrm{Deg}} = 3.4389 + 0.94591\, X_{[\mathrm{Fe}^{2+}]} + 0.15055\ X_j - 0.01689\, X_{[\mathrm{Fe}^{2+}]}\, X_j - 0.00223 \times 65\, X_{[\mathrm{Fe}^{2+}]} + 0.00004 \times 65\, X_j + 27.218 \quad (23)$$

$$Y_{\%\mathrm{Min}} = 9.9744 + 2.2037\, X_{[\mathrm{Fe}^{2+}]} + 0.55731 X_j - 0.05373\, X_{[\mathrm{Fe}^{2+}]}\, X_j - 0.00680 \times 65\, X_{[\mathrm{Fe}^{2+}]} - 0\ .00155 \times 65\, X_j + 28.992 \quad (24)$$

For both $Y_{\%Deg}$ and $Y_{\%Min}$, the variables $X_{[Fe^{2+}]}$ and X_j present antagonism in the mathematical models to the responses of the factorial design, as well as a positive effect of X_j. Other interactions of the independent variables in the $Y_{\%Deg}$, and $Y_{\%Min}$ responses can be seen in Fig. S2a and S2b, respectively, where they are present as desirability surface graphs for the factorial design of PEF.

3.4 Solar photoelectro-Fenton treatment of the GW sample

The optimum conditions defined by the observed mineralization response of the experimental design for the PEF process (78% TOC removal), namely $[Fe^{2+}]$ = 5 mg L^{-1} and j = 77.5 mA cm^{-2}, were applied to the treatment of 10 L of GW by SPEF in the pre-pilot plant. The experiments were carried out in triplicate, on a sunny day without clouds, with only natural radiation, during the most intense sunny hours (average solar intensity = 37.4 W m^{-2}) of the Brazilian summer (month of February), with a total duration of 4 h. The results are shown in Fig. 11, and demonstrate satisfactory LAS degradation profiles,

with 70% of removal of surfactant and 55% of GW mineralization after 240 min of treatment. These results are very promising to treat larger volumes of GW and achieve degradation and mineralization rates close to those obtained at bench scale, revealing that factorial design is a useful tool for optimizing H_2O_2-based EAOPs for the treatment of real wastewater. In SPEF, the average energy consumption was estimated as 0.32 (kWh (kg TOC)$^{-1}$), which can also be interpreted as the energy needed to treat 1 m^3 of an effluent containing up to 1000 mg L^{-1} of TOC. This low value is indicative of the feasibility of applying the process, if compared to results in the literature (see Table 1).

Insert Fig. 11

3.5 Acute toxicity to Artemia salina

The acute toxicity for brine shrimp was evaluated for the effluents resulting from: (a) AO-H_2O_2, fixing $X_{[LSA]}$ = 40 mg L^{-1}, X_j = 32.5 mA cm^{-2}, X_t = 120 min (52% TOC removal); (b) PEF, fixing $X_{[LSA]}$ = 40 mg L^{-1}, $X_{[Fe^{2+}]}$ = 5 mg L^{-1}, X_j = 77.5 mA cm^{-2}, X_t = 120 min (78% TOC removal); and (c) SPEF, fixing the same conditions of PEF, after 240 min of treatment (55% TOC removal). Concentrations of 12.5%, 25%, 50% and 70% (%v/v) were studied, and results were compared to GW control. The toxicity profiles in terms of mortality are depicted in Fig. 12. In all cases, they disclose the contribution of EAOPs to decrease the toxicity of GW to *A. salina* (i.e., a significant decay of mortality can be seen upon the application of EAOPs). The LC_{50}, toxicity units (TU) values and class, calculated according to Persoone et al. [58], were determined for each effluent and are shown in Table S2. Note that the different TU values for the three analyzed effluents are correlated to the TOC reduction rates observed at the end of the treatments. It can then be inferred that the toxicity of the effluent to *A. Salina* can be associated to the residual by-products when mineralization rates are <78%, and that a reduction in the LC_{50} toxicity unit of at least 18 times can be expected when mineralization rates > 52% are achieved.

These findings reinforce the idea of the feasibility of applying factorial planning to optimize EAOPs applied to the treatment of effluents with a xenobiotic character, such as GW.

Insert Fig. 12

4. Conclusions

The factorial experimental design proved to be effective for the treatment of data in the application and optimization of the EAOPs for the treatment of raw GW. However, LAS recalcitrance and mineralization resistance characterizes the effluent treated here. AO-H_2O_2 is a promising system for GW treatment, reaching satisfactory degradation and mineralization rates, which is guaranteed only by the catalytic action of the BDD anode and H_2O_2 electrogeneration at the carbonaceous cathode. On the other hand, the PEF and SPEF processes presented, even in upon replacement of the BDD by a Pt anode, greater capacity for LAS degradation and GW mineralization due to the occurrence of Fenton‘s reaction and successive photoreduction of Fe(III) complexes. SPEF process at pre-pilot scale showed a great performance for GW treatment, achieving results very similar to those obtained in bench scale optimization even for the acute toxicity reduction.

Acknowledgements

The authors wish to thank the Brazilian funding agencies Conselho Nacional de Desenvolvimento Científico e Tecnológico (CNPq), Coordenação de Aperfeiçoamento de Pessoal de Nível Superior (CAPES - Código de Financiamento 001), and Fundação de Apoio ao Desenvolvimento do Ensino, Ciência e Tecnologia do Estado de Mato Grosso do Sul (FUNDECT). Financial support from project PID2019-109291RB-I00 (MCIN/AEI/ 10.13039/501100011033, Spain) is also acknowledged.

References

[1] UNESCO – United Nations Educational, Scientific and Cultural Organization, FAO – Food and Agriculture Organization, REDE BRASIL DO PACTO GLOBAL. Relatório Mundial das Nações Unidas sobre Desenvolvimento dos Recursos Hídricos 2021 - O Valor da Água - Fatos e dados (2021). Available in: https://materiais.pactoglobal.org.br/valor-da-agua-fatos-e-dados. Last access: October 2021.

[2] S. Barışçı, O. Turkay, Domestic greywater treatment by electrocoagulation using hybrid electrode combinations, J. Water Process Eng. 10 (2016) 56-66. https://doi.org/10.1016/j.jwpe.2016.01.015

[3] A.K. Vuppaladadiyam, N. Merayo, P. Prinsen, R. Luque, A. Blanco, M. Zhao, A review on greywater reuse: quality, risks, barriers and global scenarios, Rev. Environ. Sci. Biotechnol. 18 (2019) 77-99. https://doi.org/10.1007/s11157-018-9487-9

[4] N. Liu, Z. Wu, Toxic effects of linear alkylbenzene sulfonate on Chara vulgaris L, Environ. Sci. Pollut. Res. 25 (2018) 4934-4941. https://doi.org/10.1007/s11356-017-0883-4

[5] J. Zhou, Z. Wu, D. Yu, Y. Pang, H. Cai, Y. Liu, Toxicity of linear alkylbenzene sulfonate to aquatic plant Potamogeton perfoliatus L, Environ. Sci. Pollut. Res. 25 (2018) 32303-32311. https://doi.org/10.1007/s11356-018-3204-7

[6] F. Babaei, M.H. Ehrampoush, H. Eslami, M.T. Ghaneian, H. Fallahzadeh, P. Talebi, R.F. Fard, A.A. Ebrahimi, Removal of linear alkylbenzene sulfonate and turbidity from greywater by a hybrid multi-layer slow sand filter microfiltration ultrafiltration system, J. Clean. Prod. 211 (2019) 922-931. https://doi.org/10.1016/j.jclepro.2018.11.255

[7] L. Hernández Leal, N. Vieno, H. Temmink, H., G. Zeeman, C.J. Buisman, Occurrence of xenobiotics in gray water and removal in three biological treatment systems, Environ. Sci. Technol. 44 (2010) 6835-6842. https://doi.org/10.1021/es101509e

[8] S. Tsoumachidou, T. Velegraki, A. Antoniadis, I. Poulios, Greywater as a sustainable water source: a photocatalytic treatment technology under artificial and solar illumination, J. Environ. Manage. 195 (2017) 232-241. https://doi.org/10.1016/j.jenvman.2016.08.025

[9] M. Zhang, Y. Shi, Y. Lu, A.C. Johnson, S. Sarvajayakesavalu, Z. Liu, C. Su, Y. Zhang, M.D. Juergens, X. Jin, The relative risk and its distribution of endocrine disrupting chemicals, pharmaceuticals and personal care products to freshwater organisms in the Bohai Rim, China, Sci. Total Environ. 590 (2017) 633-642. https://doi.org/10.1016/j.scitotenv.2017.03.011

[10] D.D. Ramos, P.C.S. Bezerra, F.H. Quina, R.F. Dantas, G.A. Casagrande, S.C. Oliveira, L.C.S. Oliveira, V.S. Ferreira, S.L. Oliveira, A. Machulek Jr., Synthesis and characterization of TiO_2 and TiO_2/Ag for use in photodegradation of methylviologen, with kinetic study by laser flash photolysis, Environ. Sci. Pollut. Res. 22 (2015) 774-783. https://doi.org/10.1007/s11356-014-2678-1

[11] N. Sakai, J. Shirasaka, Y. Matsui, M.R. Ramli, K. Yoshida, M.A. Mohd, M. Yoneda, Occurrence, fate and environmental risk of linear alkylbenzene sulfonate in the Langat and Selangor River basins, Malaysia, Chemosphere 172 (2017) 234-241. https://doi.org/10.1016/j.chemosphere.2016.12.139

[12] R. F. Nunes A.C.S.C. Teixeira, An overview on surfactants as pollutants of concern: Occurrence, impacts and persulfate-based remediation technologies, Chemosphere 300 (2022) 134507. https://doi.org/10.1016/j.chemosphere.2022.134507

[13] J. Martín, C. Mejías, M. Arenas, J.L. Santos, I. Aparicio, E. Alonso, Occurrence of linear alkylbenzene sulfonates, nonylphenol ethoxylates and di(2-ethylhexyl) phthalate in composting processes: Environ. Risks Sustain. 14 (2021) 186. https://doi.org/10.3390/su14010186

[14] C.F. Granatto, T.Z. Macedo, L.E. Gerosa, L.K. Sakamoto, E.L. Silva, M.B.A. Varesche, Scale-up evaluation of anaerobic degradation of linear alkylbenzene sulfonate from sanitary sewage in expanded granular sludge bed reactor, Int. Biodeter. Biodegrad. 138 (2019) 23-32. https://doi.org/10.1016/j.ibiod.2018.12.010

[15] T.S. Budikania, C. Irawan, K. Afriani, Foliatini, N. Saksono, Degradation of linear alkylbenzene sulfonate (LAS) by using multi-contact glow discharge electrolysis (m-CGDE) and Fe^{2+} ion as catalyst, J. Environ. Chem. Eng. 5 (2017) 2346-2349.

[16] H. Sakai, H. Song, R, Goto, Degradation of linear alkylbenzene sulfonate by UV/H_2O_2 process, Ozone Sci. Eng. 43 (2021) 317-323. https://doi.org/10.1016/j.jece.2017.04.025

[17] S. Lanzalaco, I. Sirés, A. Galia, M.A. Sabatino, C. Dispenza, O. Scialdone, Facile crosslinking of poly(vinylpyrrolidone) by electro-oxidation with IrO_2-based anode under potentiostatic conditions, J. Appl. Electrochem. 48 (2018) 1343-1352. https://doi.org/10.1007/s10800-018-1237-8

[18] C.A. Martínez-Huitle, M. Panizza, Electrochemical oxidation of organic pollutants for wastewater treatment, Curr. Opinion Electrochem. 11 (2018) 62-71. https://doi.org/10.1016/j.coelec.2018.07.010

[19] O. Cornejo, M.F. Murrieta, L.F. Castañeda, J.L. Nava, Characterization of the reaction environment in flow reactors fitted with BDD electrodes for use in

electrochemical advanced oxidation processes: A critical review, Electrochim. Acta 331 (2020) 135373. https://doi.org/10.1016/j.electacta.2019.135373

[20] A.P.P.P. da Rosa, R.P. Cavalcante, D.A. da Silva, L. de M. da Silva, T.F. da Silva, F. Gozzi, E. MacGlynn, A. Brady-Boyd, G.A. Casagrande, H. Wender, S.C. de Oliveira, A. Machulek Jr., H_2O_2-assisted photoelectrocatalytic degradation of Mitoxantrone using CuO nanostructured films: Identification of by-products and toxicity, Sci. Total Environ. 651 2 (2019) 2845-2856. https://doi.org/10.1016/j.scitotenv.2018.10.173

[21] C.A. Martínez-Huitle, E. Brillas, A critical review over the electrochemical disinfection of bacteria in synthetic and real wastewaters using a boron-doped diamond anode, Curr. Opin. Solid State Mater. Sci. 25 (2021) 100926. https://doi.org/10.1016/j.cossms.2021.100926

[22] C.A. Martínez-Huitle, M.A. Rodrigo, I. Sirés, O. Scialdone, Single and coupled electrochemical processes and reactors for the abatement of organic water pollutants: A critical review, Chem. Rev. 115 (2015) 13362-13407. https://doi.org/10.1021/acs.chemrev.5b00361

[23] E. Brillas, I. Sirés, M.A. Oturan, Electro-Fenton process and related electrochemical technologies based on Fenton's reaction chemistry, Chem. Rev. 109 (2009) 6570-6631. https://doi.org/10.1021/cr900136g

[24] N. Barhoumi, L. Labiadh, M.A. Oturan, N. Oturan, A. Gadri, S. Ammar, E. Brillas, Electrochemical mineralization of the antibiotic levofloxacin by electro-Fenton-pyrite process, Chemosphere 141 (2015) 250-257. https://doi.org/10.1016/j.chemosphere.2015.08.003

[25] S. Lanzalaco, I. Sirés, M.A. Sabatino, C. Dispenza, O. Scialdone, A. Galia, Synthesis of polymer nanogels by electro-Fenton process: investigation of the effect

636 of main operation parameters, Electrochim. Acta 246 (2017) 812-822.
637 https://doi.org/10.1016/j.electacta.2017.06.097
638 [26] G. Daniel, Y. Zhang, S. Lanzalaco, F. Brombin, T. Kosmala, G. Granozzi, A. Wang,
639 E. Brillas, I. Sirés, C. Durante, Chitosan-derived nitrogen-doped carbon
640 electrocatalyst for a sustainable upgrade of oxygen reduction to hydrogen peroxide
641 in UV-assisted electro-Fenton water treatment, ACS Sustain. Chem. Eng. 8 (2020)
642 14425-14440. https://doi.org/10.1021/acssuschemeng.0c04294
643 [27] V. Melin, P. Salgado, A. Thiam, A. Henríquez, H.D. Mansilla, J. Yáñez, C. Salazar,
644 Study of degradation of amitriptyline antidepressant by different electrochemical
645 advanced oxidation processes, Chemosphere 274 (2021) 129683.
646 https://doi.org/10.1016/j.chemosphere.2021.129683
647 [28] I. Sirés, E. Brillas, Upgrading and expanding the electro-Fenton and related
648 processes, Curr. Opin. Electrochem. 27 (2021) 100686.
649 https://doi.org/10.1016/j.coelec.2020.100686
650 [29] D.R. Guelfi, E. Brillas, F. Gozzi, A. Machulek Jr, S.C. de Oliveira, I. Sirés,
651 Influence of electrolysis conditions on the treatment of herbicide bentazon using
652 artificial UVA radiation and sunlight. Identification of oxidation products, J.
653 Environ. Manage. 231 (2019) 213-221.
654 https://doi.org/10.1016/j.jenvman.2018.10.029
655 [30] Y. Zhang, A. Wang, S. Ren, Z. Wen, X. Tian, D. Li, J. Li, Effect of surface
656 properties of activated carbon fiber cathode mineralization of antibiotic cefalexin
657 by electro-Fenton and photoelectro-Fenton treatments: Mineralization, kinetics and
658 oxidation products, Chemosphere 221 (2019) 423-432.
659 https://doi.org/10.1016/j.chemosphere.2019.01.016

660 [31] Y. Zhang, G. Daniel, S. Lanzalaco, A.A. Isse, A. Facchin, A. Wang, E. Brillas, C.
661 Durante, I. Sirés, H_2O_2 production at gas-diffusion cathodes made from agarose-
662 derived carbons with different textural properties for acebutolol degradation in
663 chloride media, J. Hazard. Mater. 423 (2022) 127005.
664 https://doi.org/10.1016/j.jhazmat.2021.127005
665 [32] D.R.V. Guelfi, F. Gozi, A. Machulek Jr., I. Sirés, E. Brillas, S.C. de Oliveira,
666 Degradation of herbicide S-metolachlor by electrochemical AOPs using a boron-
667 doped diamond anode, Catal. Today 313 (2018) 182-188.
668 https://doi.org/10.1016/j.cattod.2017.10.026
669 [33] D.H. Funai, F. Didier, J. Giménez, S. Esplugas, P. Marco, A. Machulek Jr., Photo-
670 Fenton treatment of valproate under UVC, UVA and simulated solar radiation, J.
671 Hazard. Mater. 323 (2017) 537-549. https://doi.org/10.1016/j.jhazmat.2016.06.034
672 [34] A.J. Luna, O. Chiavone-Filho, A. Machulek Jr., J.E.F. de Moraes, C.A.O.
673 Nascimento, Photo-Fenton oxidation of phenol and oganochlorides (2,4-DCP and
674 2,4-D) in aqueous alkaline medium with high chloride concentration, J. Environ.
675 Manage. 111 (2012) 10-17. https://doi.org/10.1016/j.jenvman.2012.06.014
676 [35] R. Salazar, J. Gallardo-Arriaza, J. Vidal, C. Rivero-Vera, C. Toledo-Neira, M.A.
677 Sandoval, L. Cornejo-Ponce, A. Thiam, Treatment of industrial textile wastewater
678 by the solar photoelectro-Fenton process: Influence of solar radiation and applied
679 current, Solar Energy 190 (2019) 82-91.
680 https://doi.org/10.1016/j.solener.2019.07.072
681 [36] M.F. Murrieta, I. Sirés, E. Brillas, J.L. Nava, Mineralization of Acid Red 1 azo dye
682 by solar photoelectro-Fenton-like process using electrogenerated HClO and
683 photoregenerated Fe(II), Chemosphere 246 (2020) 125697.
684 https://doi.org/10.1016/j.chemosphere.2019.125697

685 [37] L.D.M. da Silva, R.P. Cavalcante, R.F. Cunha, F. Gozzi, R.F. Dantas, S.C. de
686 Oliveira, A.M. Junior,
687 acid degradation by direct photolysis and the UV-ABC/H_2O_2 process: factorial design,
688 kinetics, identification of intermediates, and toxicity evaluation, Sci. Total Environ.
689 573 (2016) 518-531. https://doi.org/10.1016/j.scitotenv.2016.08.139
690 [38] G.E.P. Box, J.S. Hunter, W.G. Hunter, Statistics for Experiments: Design,
691 Innovation, and Discovery, 2nd. Ed. John Wiley & Sons, Inc. Hoboken, New
692 Jersey, 2022.
693 [39] D.A. da Silva, R.P. Cavalcante, R.F. Cunha, A.M. Junior, S.C. de Oliveira,
694 Optimization of nimesulide oxidation via a UV-ABC/H_2O_2 treatment process:
695 degradation products, ecotoxicological effects, and their dependence on the water
696 matrix, Chemosphere 207 (2018) 457-468.
697 https://doi.org/10.1016/j.chemosphere.2018.05.115
698 [40] L. Xu, S. Yang, Y. Zhang, Z. Jin, X. Huang, K. Bei, M. Zhao, H. Kong, X. Zheng,
699 A hydroponic green roof system for rainwater collection and greywater treatment,
700 J. Clean. Prod. 261 (2020) 121132. https://doi.org/10.1016/j.jclepro.2020.121132
701 [41] M.F. Costa, A.M. de Oliveira, E.N. de O. Junior, Biodegradation of linear
702 alkylbenzene sulfonate (LAS) by *Penicillium chrysogenum*, Biores. Technol.
703 Reports 9 (2020) 100363. https://doi.org/10.1016/j.biteb.2019.100363
704 [42] B. Bakheet, V. Prodanovic, A. Deletic, D. McCarthy, Effective treatment of
705 greywater via green wall biofiltration and electrochemical disinfection, Water Res.
706 185 (2020) 116228. https://doi.org/10.1016/j.watres.2020.116228
707 [43] E.D.A. do Couto, M.L. Calijuri, P.P. Assemany, A. da F. Santiago, L.S. Lopes,
708 Greywater treatment in airports using anaerobic filter followed by UV disinfection:

709 an efficient and low cost alternative, J. Clean. Prod. 106 (2015) 372-379.
710 http://dx.doi.org/10.1016/j.jclepro.2014.07.065
711 [44] S. Kim, C. Park, Potential of ceramic ultrafiltration membranes for the treatment of
712 anionic surfactants in laundry wastewater for greywater reuse, J. Water Process
713 Eng. 44 (2021) 102373. https://doi.org/10.1016/j.jwpe.2021.102373
714 [45] K.S. Oh, P.E. Poh, M.N. Chong, D. Gouwanda, W.H. Lam, C.Y. Chee, Optimizing
715 the in-line ozone injection and delivery strategy in a multistage pilot-scale
716 greywater treatment system: System validation and cost-benefit analysis, J.
717 Environ. Chem. Eng. 3 (2015) 1146-1151.
718 https://doi.org/10.1016/j.jece.2015.04.022
719 [46] E.L. Terechova, G. Zhang, J. Chen, N.A. Sosnina, F. Yang, Combined chemical
720 coagulation–flocculation/ultraviolet photolysis treatment for anionic surfactants in
721 laundry wastewater, J. Environ. Chem. Eng. 2 (2014) 2111-2119.
722 https://doi.org/10.1016/j.jece.2014.09.011
723 [47] P. Patel, S. Gupta, P. Mondal, Electrocoagulation process for greywater treatment:
724 Statistical modeling, optimization, cost analysis and sludge management, Sep.
725 Purif. Technol. (2022) 121327. https://doi.org/10.1016/j.seppur.2022.121327
726 [48] A. K. Mostafazadeha, A. T. Benguita, A. Carabina, P. Droguia, E. Brienb,
727 Development of combined membrane filtration, electrochemical technologies, and
728 adsorption processes for treatment and reuse of laundry wastewater and removal of
729 nonylphenol ethoxylates as surfactants, J. Water Process Eng. 28 (2019) 277-292.
730 https://doi.org/10.1016/j.jwpe.2019.02.014
731 [49] F. Ghanbari, C.A. Martínez-Huitle, Electrochemical advanced oxidation processes
732 coupled with peroxymonosulfate for the treatment of real washing machine

effluent: a comparative study, J. Electroanal. Chem. 847 (2019) 113182. https://doi.org/10.1016/j.jelechem.2019.05.064

[50] K. Thirugnanasambandham, V. Sivakumar, Optimization of treatment of grey wastewater using Electro-Fenton technique–Modeling and validation, Process Saf. Environ. Prot. 95 (2015) 60-68. https://doi.org/10.1016/j.psep.2015.02.001

[51] APHA, Standard Methods for the Examination of Water and Wastewater, 23nd Ed., American Public Health Association (APHA), New York, 2017.

[52] E. Jurado, M. Fernández-Serrano, J. Núñez-Olea, G. Luzón, M. Lechuga, Simplified spectrophotometric method using methylene blue for determining anionic surfactants: applications to the study of primary biodegradation in aerobic screening tests, Chemosphere 65 (2006) 278-285. https://doi.org/10.1016/j.chemosphere.2006.02.044

[53] S. Mohajeri, H.A. Aziz, M.H. Isa, M.A. Zahed, M.N. Adlan, Statistical optimization of process parameters for landfill leachate treatment using electro-Fenton technique, J. Hazard. Mater. 176(1-3) (2010) 749-758. https://doi.org/10.1016/j.jhazmat.2009.11.099

[54] F. Alcaide, G. Álvarez, D.R. Guelfi, E. Brillas, I Sirés, A stable CoSP/MWCNTs air-diffusion cathode for the photoelectro-Fenton degradation of organic pollutants at pre-pilot scale, Chem. Eng. J. 379 (2020) 122417. https://doi.org/10.1016/j.cej.2019.122417

[55] T. Mesarič, C. Gambardella, T. Milivojević, M. Faimali, D. Drobne, C. Falugi, M. Darko, A. Jemed, K. Sepčić, High surface adsorption properties of carbon-based nanomaterials are responsible for mortality, swimming inhibition, and biochemical responses in Artemia salina larvae, Aquat. Toxicol. 163 (2015) 121-129. https://doi.org/10.1016/j.aquatox.2015.03.014

[56] J.P. Kushwaha, V.C. Srivastava, I.D. Mall, Organics removal from dairy wastewater by electrochemical treatment and residue disposal. Sep. Purif. Technol. 76 (2) (2010) 198-205. https://doi.org/10.1016/j.seppur.2010.10.008

[57] S.O. Ganiyu, C.A. Martínez-Huitle, M.A. Oturan, Electrochemical advanced oxidation processes for wastewater treatment: Advances in formation and detection of reactive species and mechanisms, Curr. Opin. Electrochem. 27 (2021) 100678. https://doi.org/10.1016/j.coelec.2020.100678

[58] G. Persoone, B. Marsalek, I. Blinova, A. Torkokne, D. Zarina, L. Manusadzianas, G. Nalecz-Jawecki, L. Tofan, N. Stepanova, L. Tothova, B. Kolar, A practical and user-friendly toxicity classification system with microbiotests for natural waters and wastewaters, Environ. Toxicol. 18 (2003) 395-402. https://doi.org/10.1002/tox.10141

Figure captions

Fig. 1. Scheme that describes the main reactions that characterize the EAOPs. AO-H_2O_2: (1), (3), (4) and (7); EF: reactions of AO-H_2O_2 plus (5) and (6); PEF: reactions of EF plus (10) and (11); and parasitic reactions: (2), (8) and (9).

Fig. 2. (a) Scheme of the bench-scale degradation system indicating the position of the main elements: 1 – Jacketed undivided cell of 150 mL capacity; 2 – Boron-doped diamond (BDD) or platinum anodes (both of 3 cm^2 geometrical active area); 3 – Air-diffusion cathode with activated carbon cloth-PTFE membrane (3 cm^2 geometrical active area); 4 – Air pump operating at 1 L min^{-1}; 5 – High precision power source operated in continuous current mode; 6 – Blacklight tube lamp (4 W, placed at 6 cm above the solution surface); 7 – Magnetic stirring bar. (b) Scheme of the pilot backflow unit used in SPEF process, indicating the position of the main elements: 1 – 20-L reservoir tank; 2 – Centrifugal pump; 3 – Rotameter type fluxometer (180 L min^{-1}); 4 – Heat-exchanger (x2); 5 – Filter-press electrochemical cell; 6 – Air pump operating at 2 L min^{-1}; 7 – Precision power source with fine adjustment; 8 – Compound Parabolic Collector (CPC) photoreactor illuminated with natural solar light.

Fig. 3. Residual plots for the percentage response of: (a) LAS degradation ($Y_{\%Deg}$, R^2 = 99.978% and R^2_{adj} = 99.89%) and (b) GW mineralization (R^2 = 99.975% and R^2_{adj} = 99.875%) obtained experimentally (blue points) by AO-H_2O_2 process, as compared to the polynomial mathematical model of prediction (red lines).

Fig. 4. Pareto charts showing the effect (and synergism) of the independent variables chosen for the experimental design on the responses of: (a) LAS degradation and (b) GW mineralization, in the AO-H_2O_2 treatment.

Fig. 5. Desirability of independent variables on the responses of: (a) $Y_{\%Deg}$ and (b) $Y_{\%Min}$, corresponding to the factorial design developed for the AO-H_2O_2 treatment of GW with 0.050 M Na_2SO_4.

Fig. 6. Surface response of the most significant interactions between the independent variables for: (a) LAS degradation (at X_t = 65 min) and (b) GW mineralization (at X_j = 55 mA cm^{-2}), corresponding to the AO-H_2O_2 treatment using a carbon-PTFE air-diffusion cathode and a Si|BDD anode in the presence of 0.050 M Na_2SO_4.

Fig. 7. Residual plots for the percentage response of: (a) LAS degradation ($Y_{\%Deg}$ R^2 = 99.337% and R^2_{adj} = 97.79%) and (b) GW mineralization ($Y_{\%Min}$, R^2 = 98.708% and R^2_{adj} = 96.771%) obtained experimentally (blue points) by PEF process, as compared to the polynomial mathematical model of prediction (red lines).

Fig. 8. Pareto charts showing the effect (and synergism) of the independent variables chosen for the experimental design on the responses of: (a) LAS degradation and (b) GW mineralization, in the PEF treatment.

Fig. 9. Desirability of independent variables on the responses of: (a) $Y_{\%Deg}$ and (b) $Y_{\%Min}$, corresponding to the factorial design developed for the PEF treatment of GW with 0.050 M Na_2SO_4.

Fig. 10. Surface response of the most significant interactions between the independent variables for: (a) LAS degradation (at X_t = 65 min) and (b) GW mineralization (at X_j = 55 mA cm^{-2}), corresponding to the PEF treatment using a carbon-PTFE air-diffusion cathode and a 4 W UVA black light tube lamp in the presence of 0.050 M Na_2SO_4.

Fig. 11. Normalized LAS and TOC decays vs. time for the SPEF treatment of the GW with 0.050 M Na_2SO_4 and 5 mg L^{-1} Fe^{2+} at pH 3.0. The pre-pilot plant comprised a CPC solar photoreactor coupled to a filter-press cell, equipped with a platinum foil as the anode and a carbon-PTFE air-diffusion cathode, both of 20 cm^2 area.

Fig. 12. Acute toxicity profiles for raw GW and for effluents generated upon treatment by different optimized EAOPs, employing *A. salina* as the indicator organism.

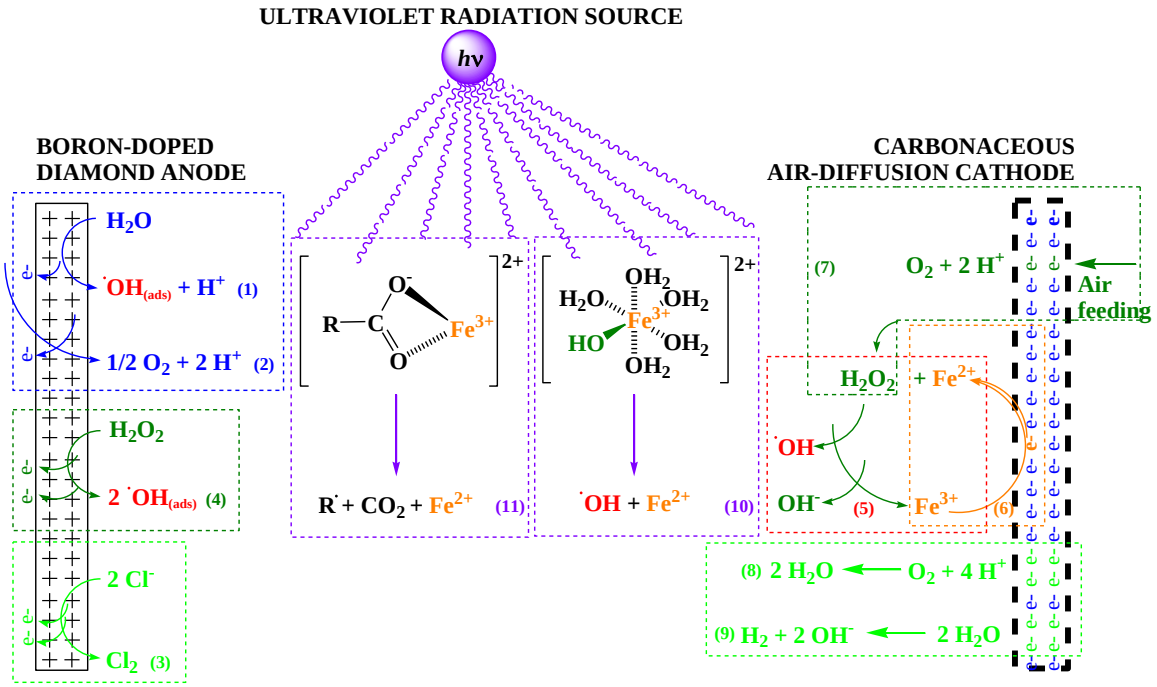
ULTRAVIOLET RADIATION SOURCE
hν
BORON-DOPED
DIAMOND ANODE
CARBONACEOUS
AIR-DIFFUSION CATHODE
H2O
·OH(ads) + H+ (1)
1/2 O2 + 2 H+ (2)
H2O2
2 ·OH(ads) (4)
2 Cl-
Cl2 (3)
R·
Fe3+
2+
R· + CO2 + Fe2+ (11)
OH2
H2O
HO
·OH + Fe2+ (10)
(7)
O2 + 2 H+
Air
feeding
H2O2
+ Fe2+
·OH
OH-
(5)
Fe3+
(6)
(8) 2 H2O
O2 + 4 H+
(9) H2 + 2 OH-
2 H2O

Fig. 1

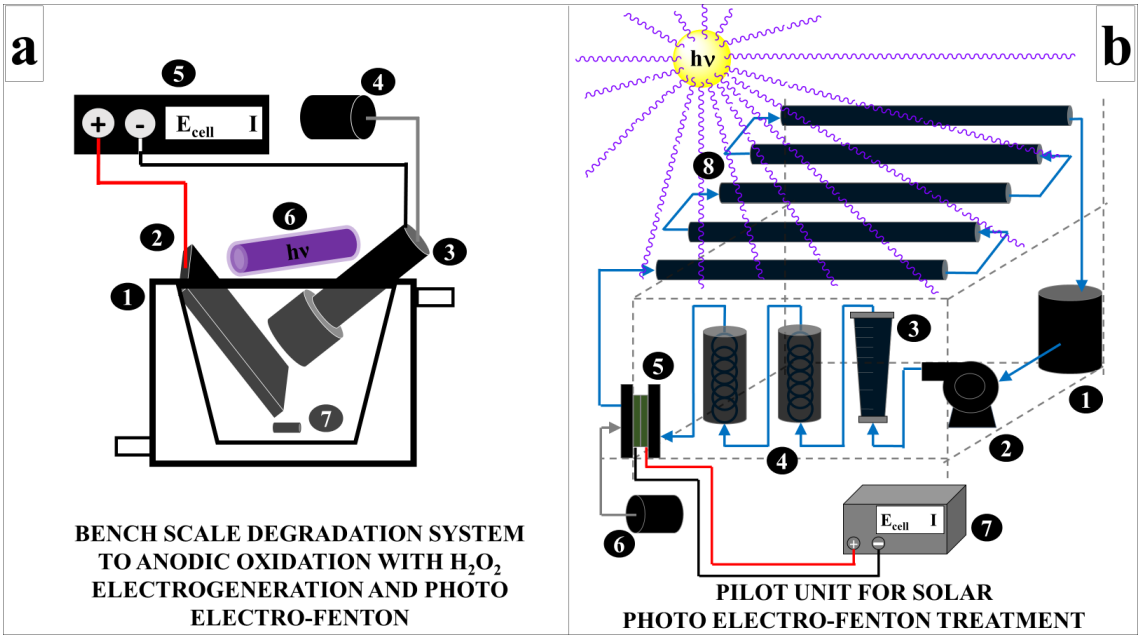
a
5
4
+
-
E cell
I
6
hν
2
3
1
7
BENCH SCALE DEGRADATION SYSTEM TO ANODIC OXIDATION WITH H2O2 ELECTROGENERATION AND PHOTO ELECTRO-FENTON
b
hν
8
3
5
1
4
2
6
E cell
I
7
PILOT UNIT FOR SOLAR PHOTO ELECTRO-FENTON TREATMENT

Fig. 2

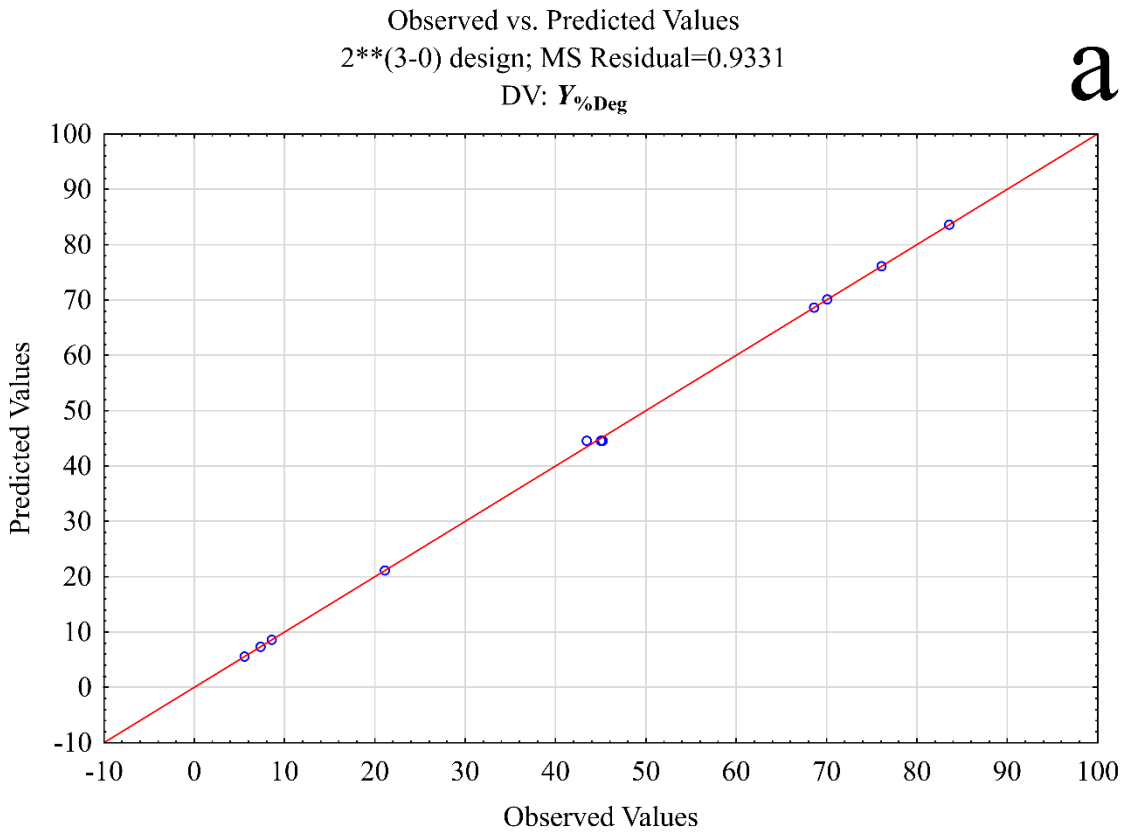
Observed vs. Predicted Values
2**(3-0) design; MS Residual=0.9331
DV: Y%Deg
a
Predicted Values
Observed Values
100
90
80
70
60
50
40
30
20
10
0
-10
-10
0
10
20
30
40
50
60
70
80
90
100

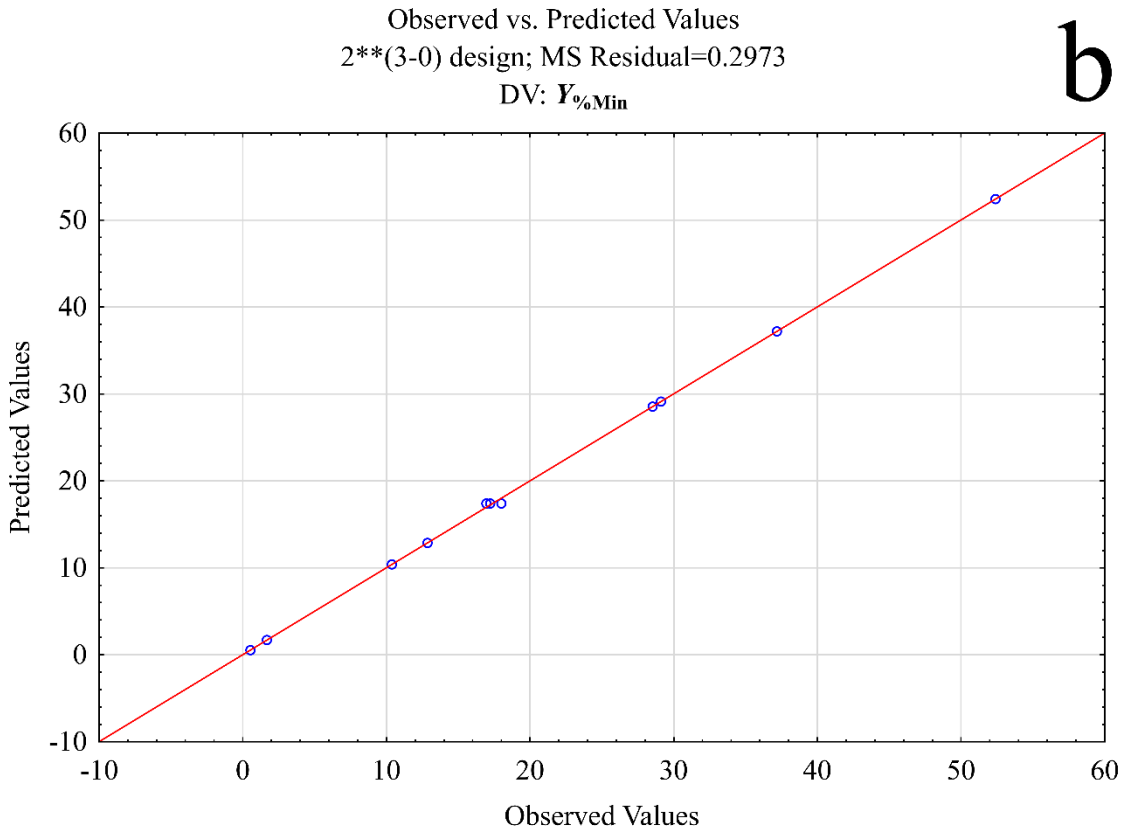
Observed vs. Predicted Values
2**(3-0) design; MS Residual=0.2973
DV: Y%Min
b
Predicted Values
Observed Values
60
50
40
30
20
10
0
-10
-10
0
10
20
30
40
50
60

Fig. 3

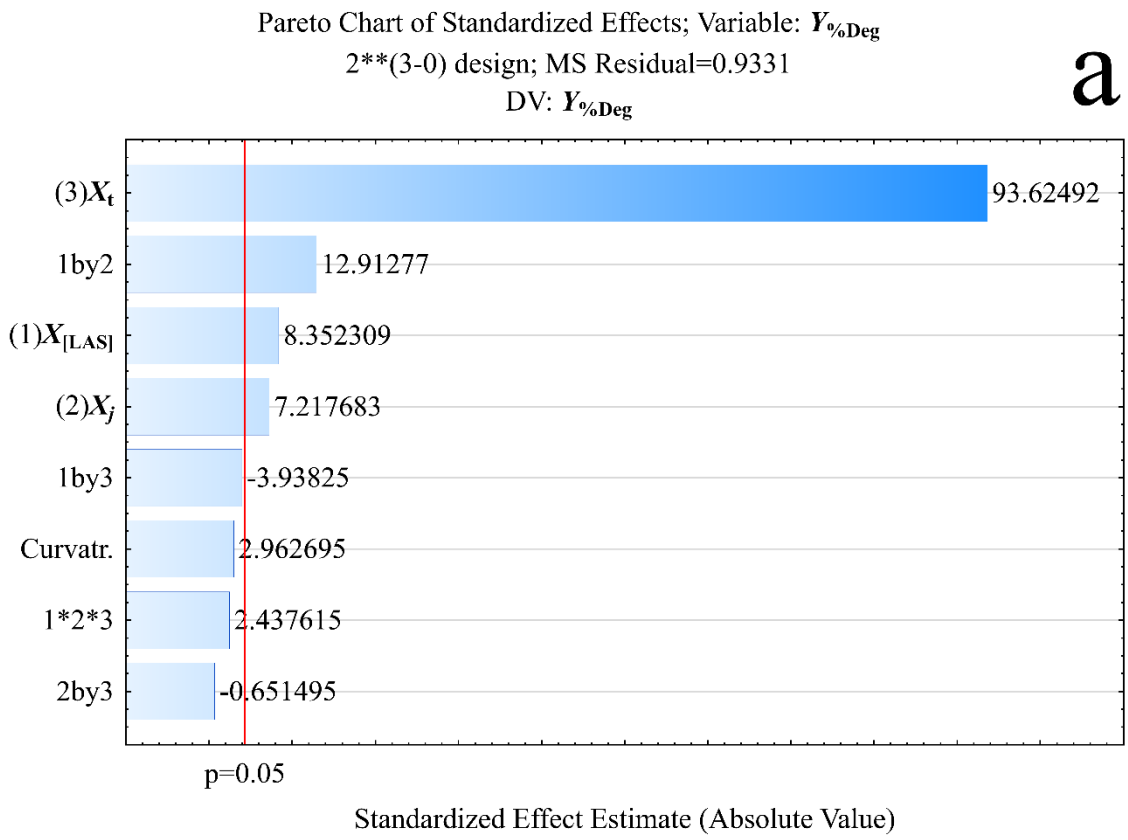
Pareto Chart of Standardized Effects; Variable: $Y_{\%Deg}$
2**(3-0) design; MS Residual=0.9331
DV: $Y_{\%Deg}$
a
(3)X_t
1by2
(1)$X_{[LAS]}$
(2)X_j
1by3
Curvatr.
1*2*3
2by3
93.62492
12.91277
8.352309
7.217683
-3.93825
2.962695
2.437615
-0.651495
p=0.05
Standardized Effect Estimate (Absolute Value)

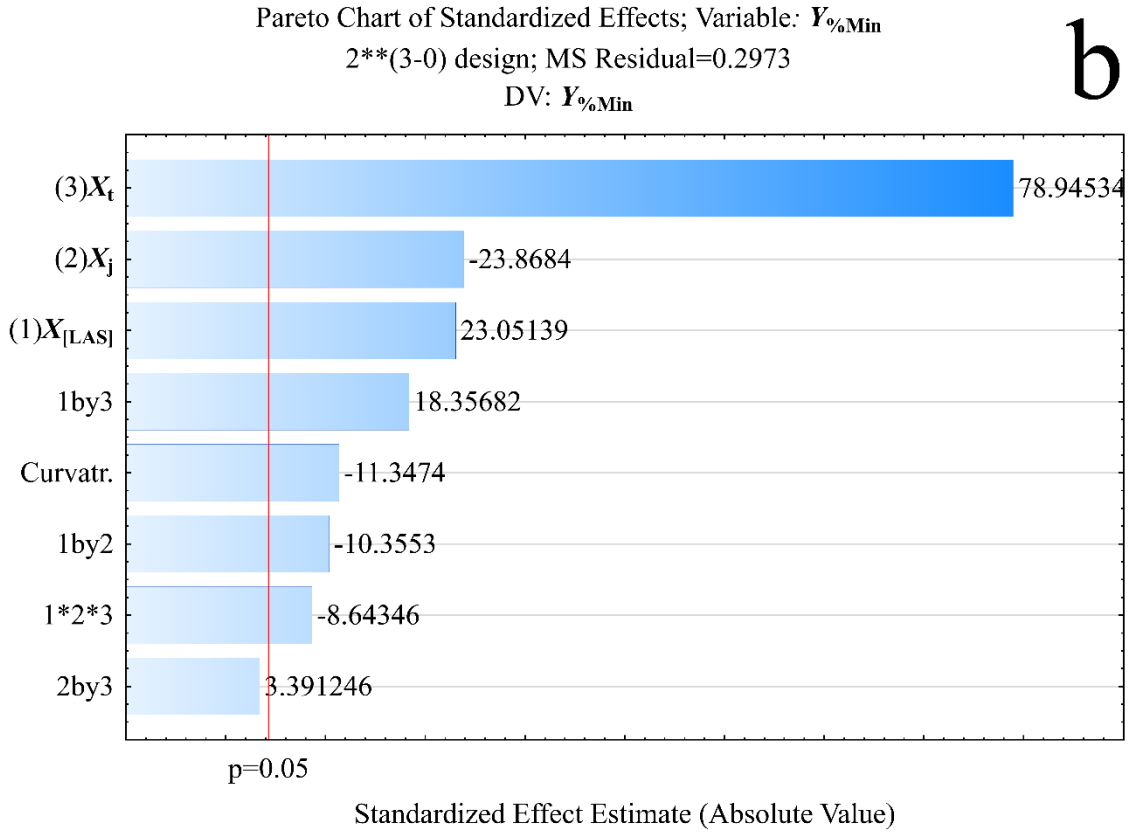
Pareto Chart of Standardized Effects; Variable: $Y_{\%Min}$
2**(3-0) design; MS Residual=0.2973
DV: $Y_{\%Min}$
b
(3)X_t
(2)X_j
(1)$X_{[LAS]}$
1by3
Curvatr.
1by2
1*2*3
2by3
78.94534
-23.8684
23.05139
18.35682
-11.3474
-10.3553
-8.64346
3.391246
p=0.05
Standardized Effect Estimate (Absolute Value)

Fig. 4

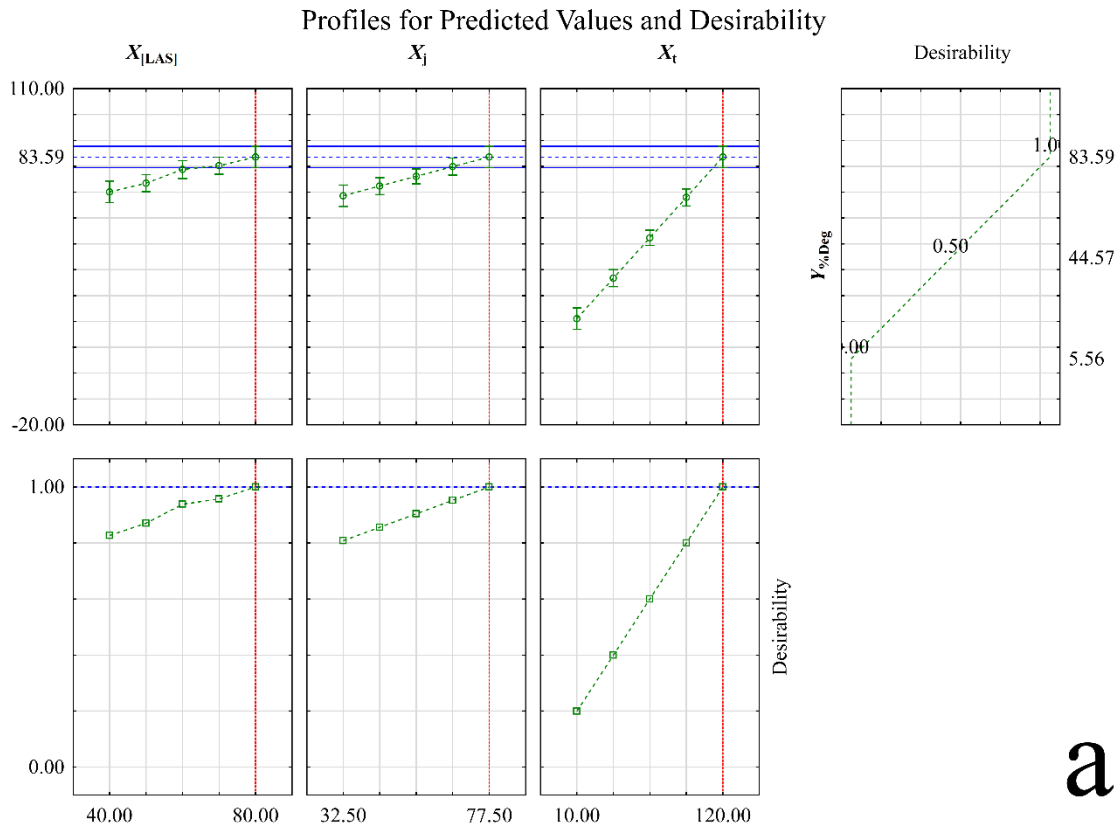
Profiles for Predicted Values and Desirability
X[LAS]
Xj
Xt
Desirability
110.00
83.59
-20.00
1.00
0.00
Desirability
1.0
0.50
.00
Y%Deg
83.59
44.57
5.56
40.00
80.00
32.50
77.50
10.00
120.00

a

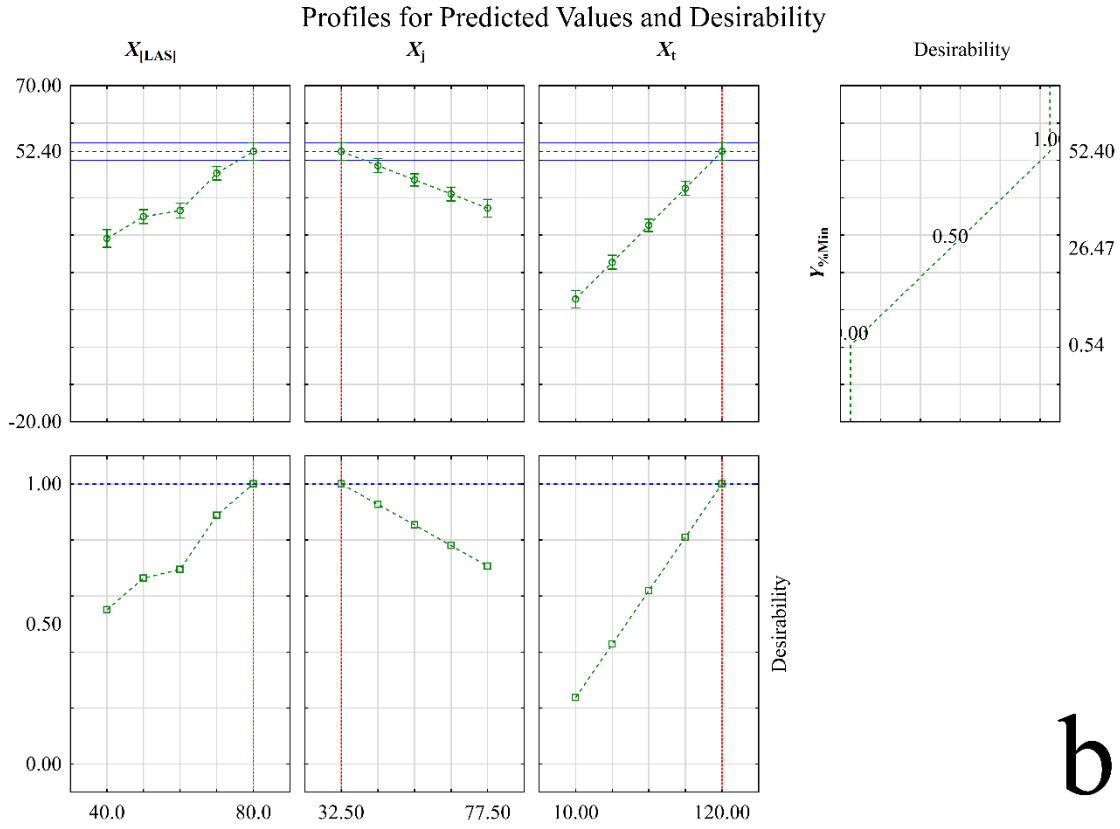
Profiles for Predicted Values and Desirability
X[LAS]
Xj
Xt
Desirability
70.00
52.40
-20.00
1.00
0.50
0.00
Desirability
1.0
0.50
.00
Y%Min
52.40
26.47
0.54
40.0
80.0
32.50
77.50
10.00
120.00

b

Fig. 5

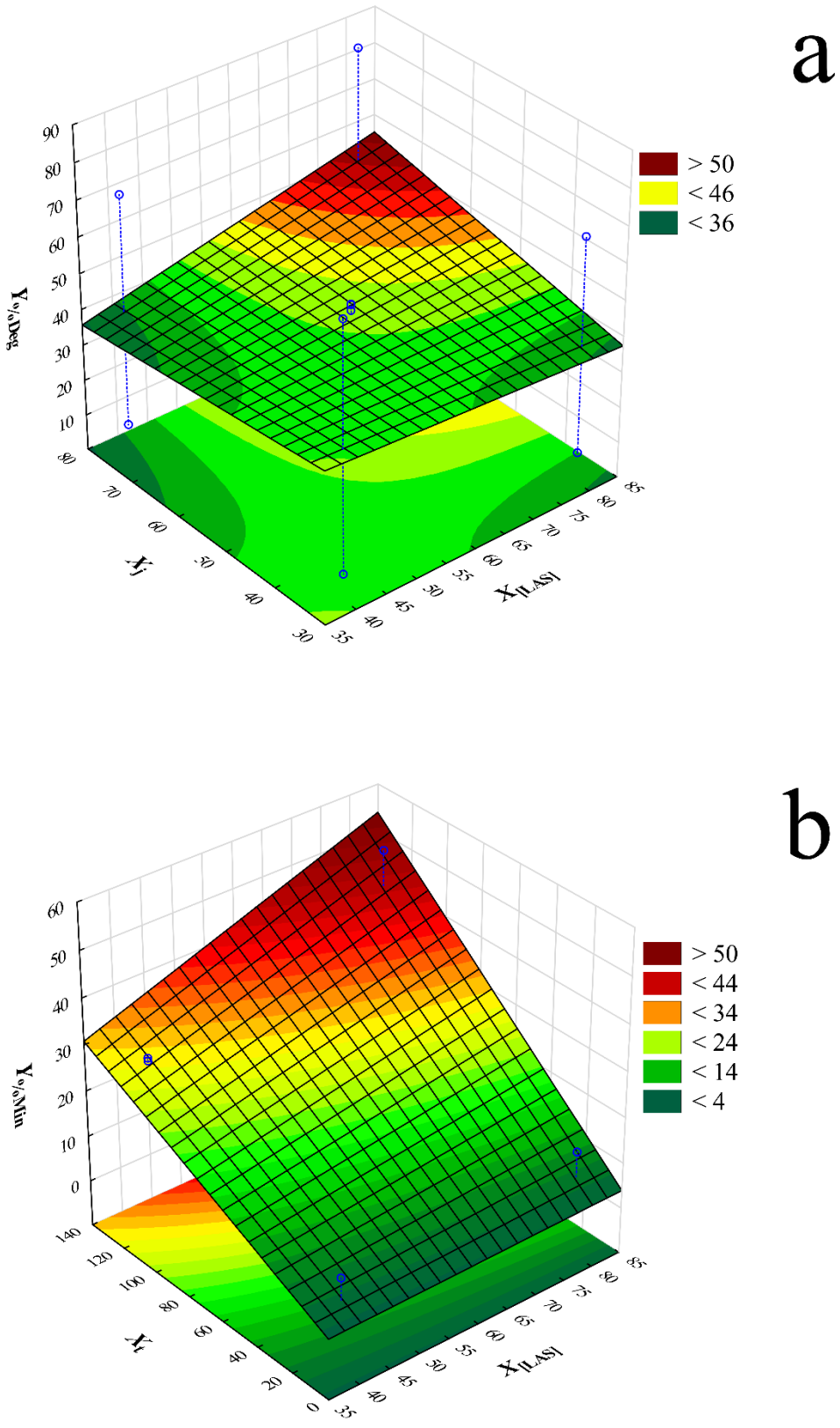

Fig. 6

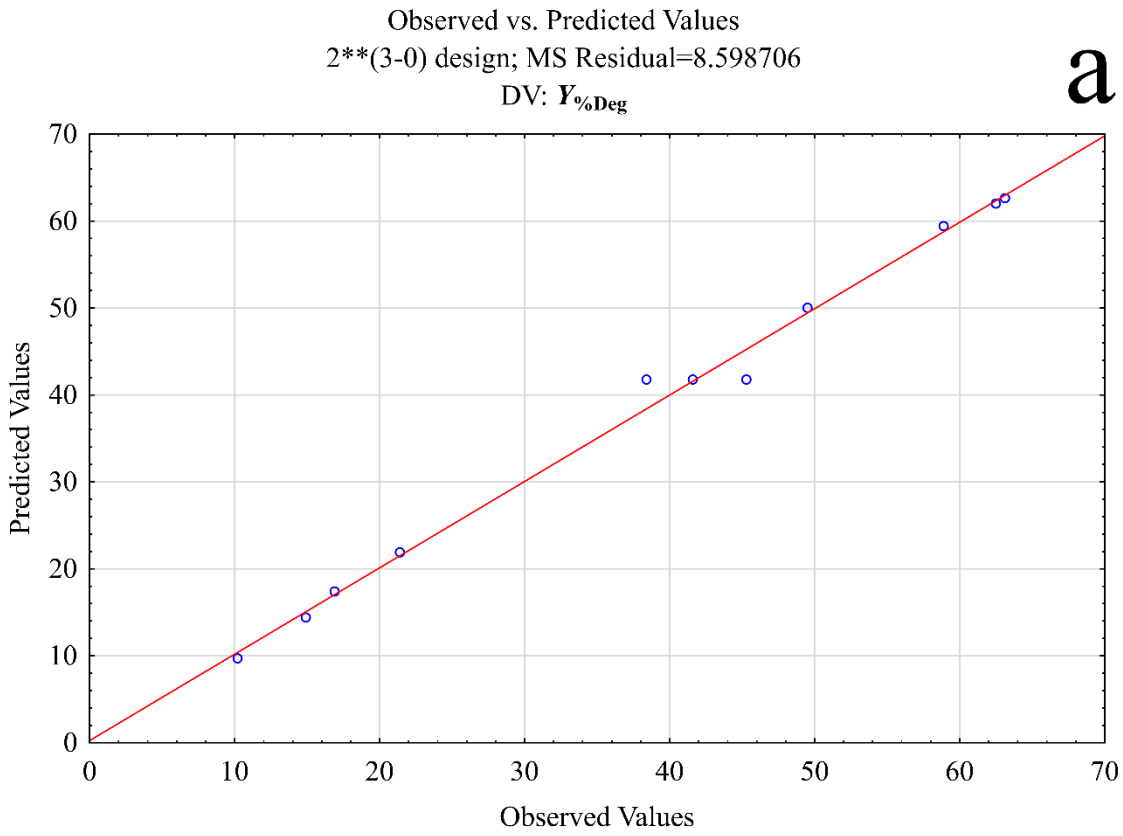
Observed vs. Predicted Values
2**(3-0) design; MS Residual=8.598706
DV: $Y_{\%Deg}$
a
Predicted Values
Observed Values
0
10
20
30
40
50
60
70

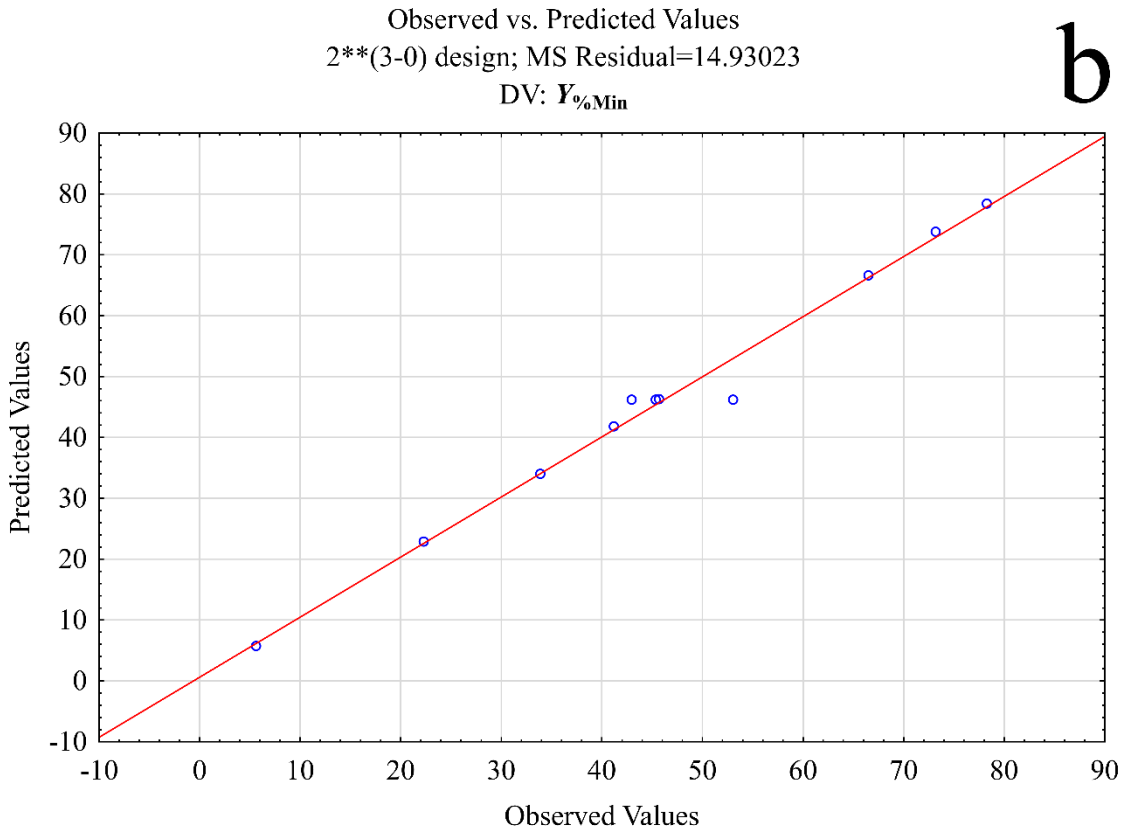
Observed vs. Predicted Values
2**(3-0) design; MS Residual=14.93023
DV: $Y_{\%Min}$
b
Predicted Values
Observed Values
-10
0
10
20
30
40
50
60
70
80
90

Fig. 7

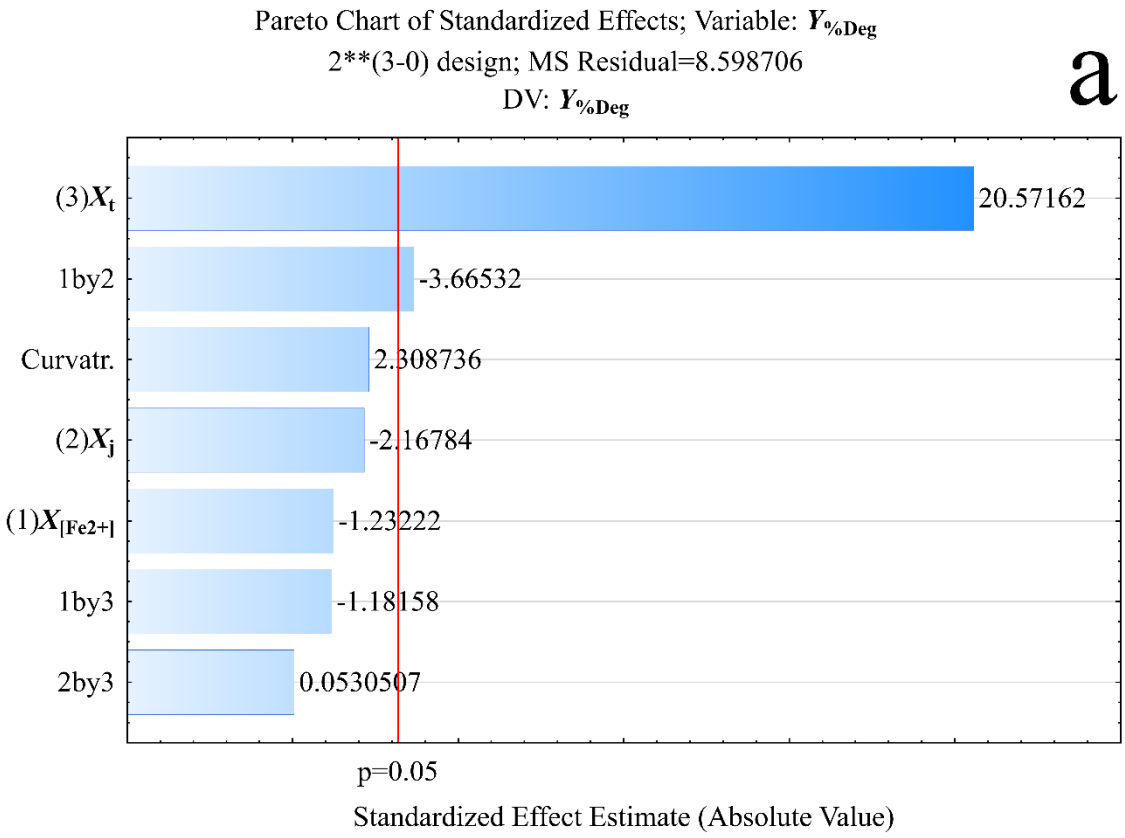
Pareto Chart of Standardized Effects; Variable: $Y_{\%Deg}$
2**(3-0) design; MS Residual=8.598706
DV: $Y_{\%Deg}$
a
(3)X_t
1by2
Curvatr.
(2)X_j
(1)$X_{[Fe2+]}$
1by3
2by3
20.57162
-3.66532
2.308736
-2.16784
-1.23222
-1.18158
0.0530507
p=0.05
Standardized Effect Estimate (Absolute Value)

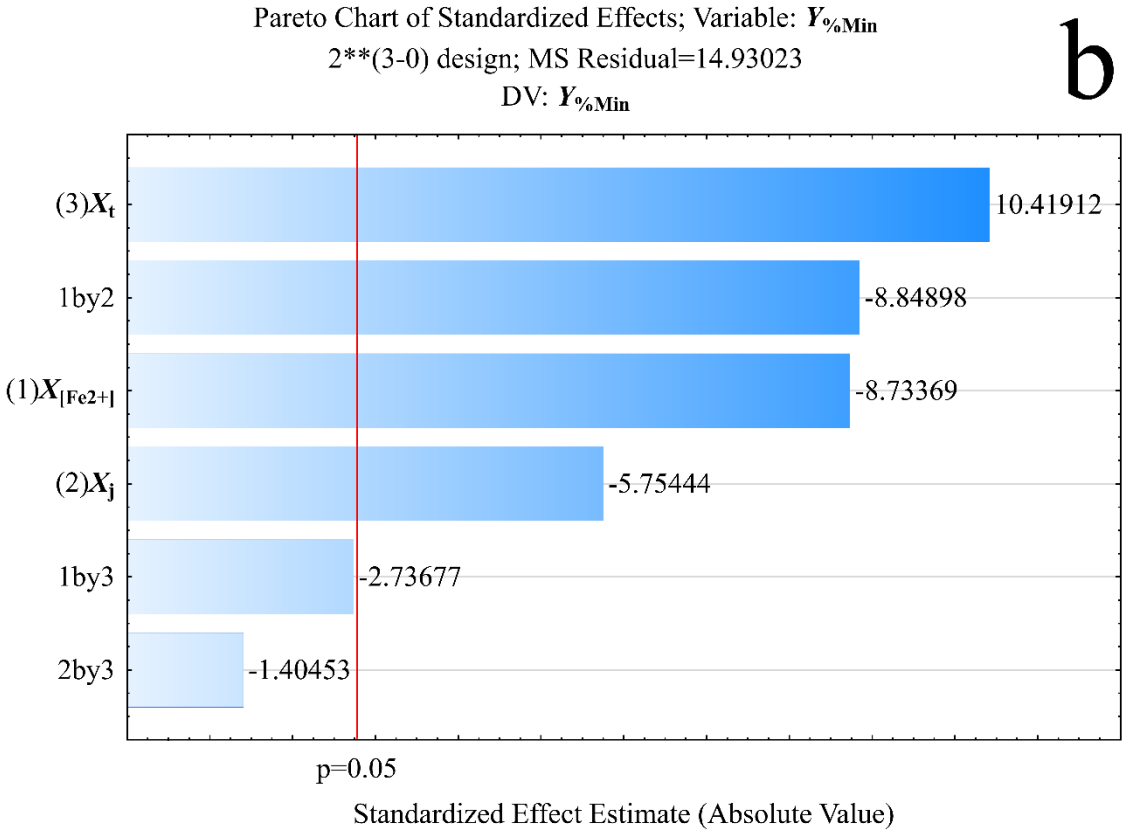
Pareto Chart of Standardized Effects; Variable: $Y_{\%Min}$
2**(3-0) design; MS Residual=14.93023
DV: $Y_{\%Min}$
b
(3)X_t
1by2
(1)$X_{[Fe2+]}$
(2)X_j
1by3
2by3
10.41912
-8.84898
-8.73369
-5.75444
-2.73677
-1.40453
p=0.05
Standardized Effect Estimate (Absolute Value)

Fig. 8

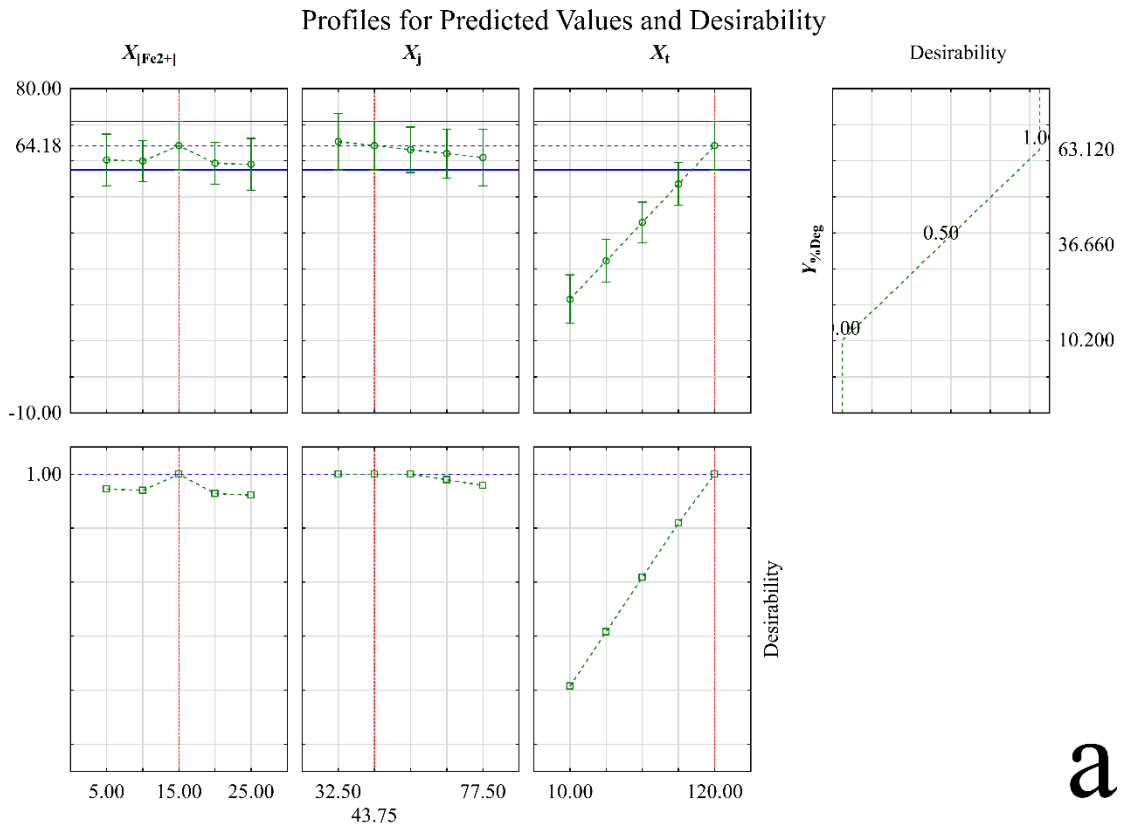
Profiles for Predicted Values and Desirability
X[Fe2+]
Xj
Xt
Desirability
80.00
64.18
-10.00
1.00
Desirability
63.120
36.660
10.200
0.50
Y%Deg
5.00
15.00
25.00
32.50
43.75
77.50
10.00
120.00

a

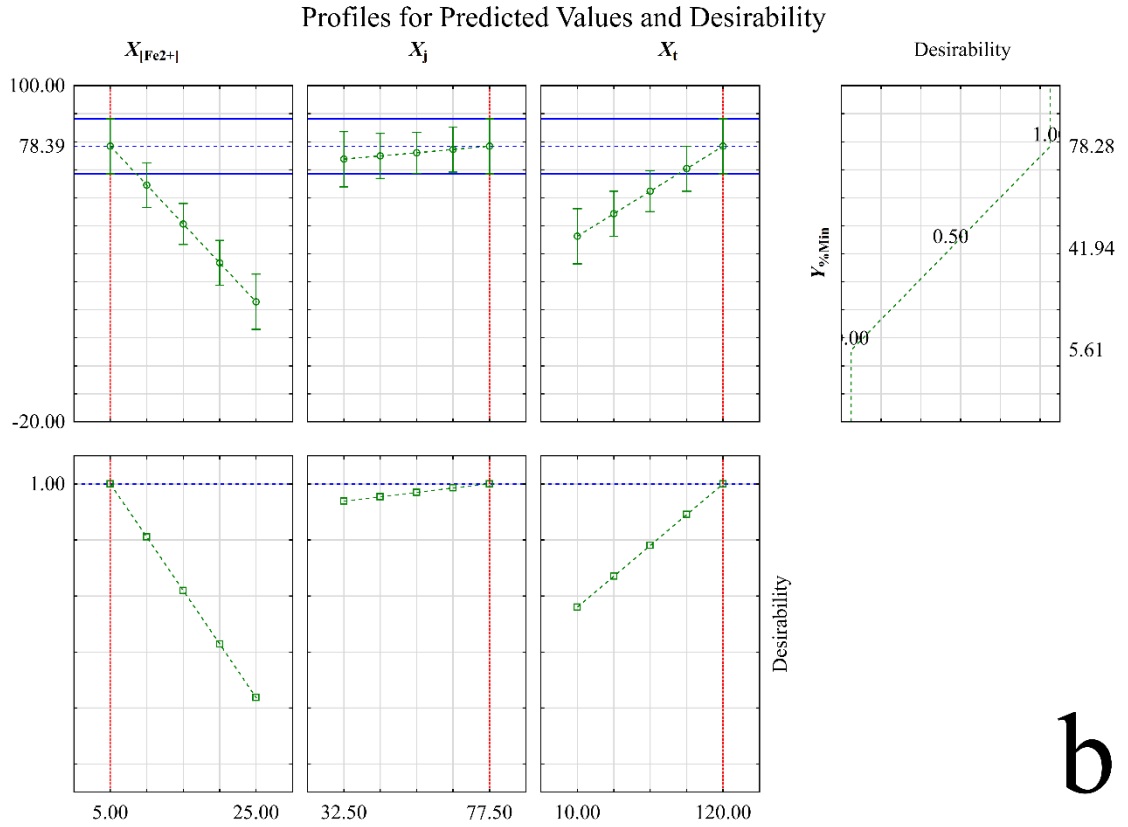
Profiles for Predicted Values and Desirability
X[Fe2+]
Xj
Xt
Desirability
100.00
78.39
-20.00
1.00
Desirability
78.28
41.94
5.61
0.50
Y%Min
5.00
25.00
32.50
77.50
10.00
120.00

b

Fig. 9

a

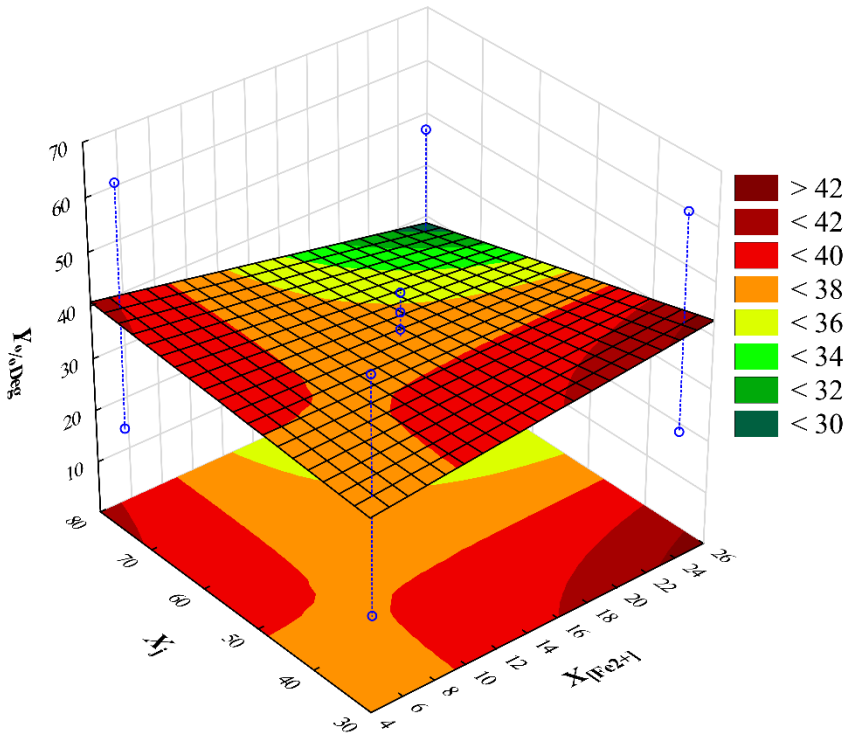
Y%Deg
X[Fe2+]
Xj
> 42
< 42
< 40
< 38
< 36
< 34
< 32
< 30

b

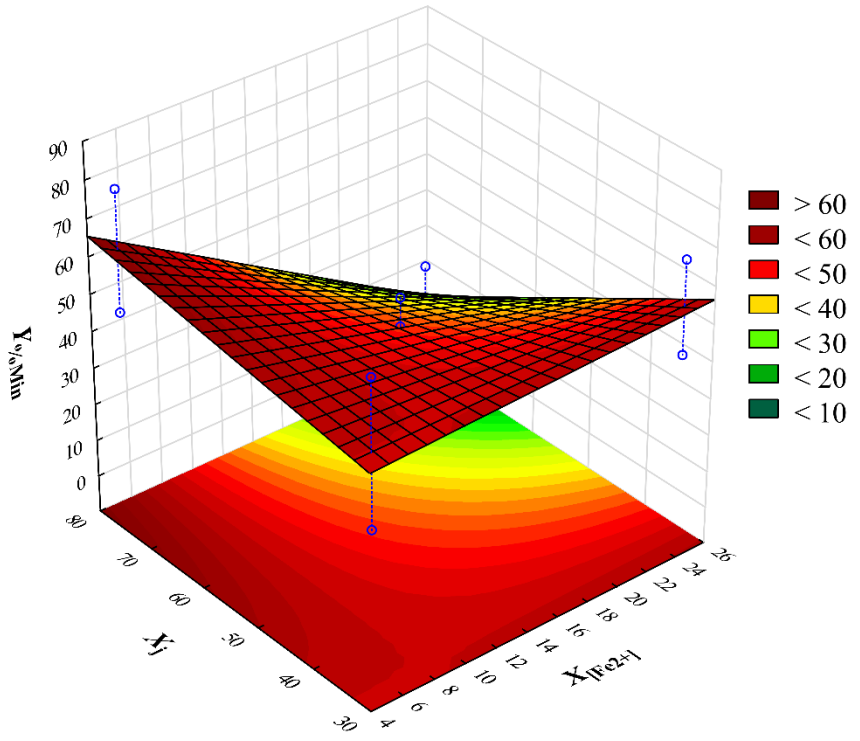
Y%Min
X[Fe2+]
Xj
> 60
< 60
< 50
< 40
< 30
< 20
< 10

Fig. 10

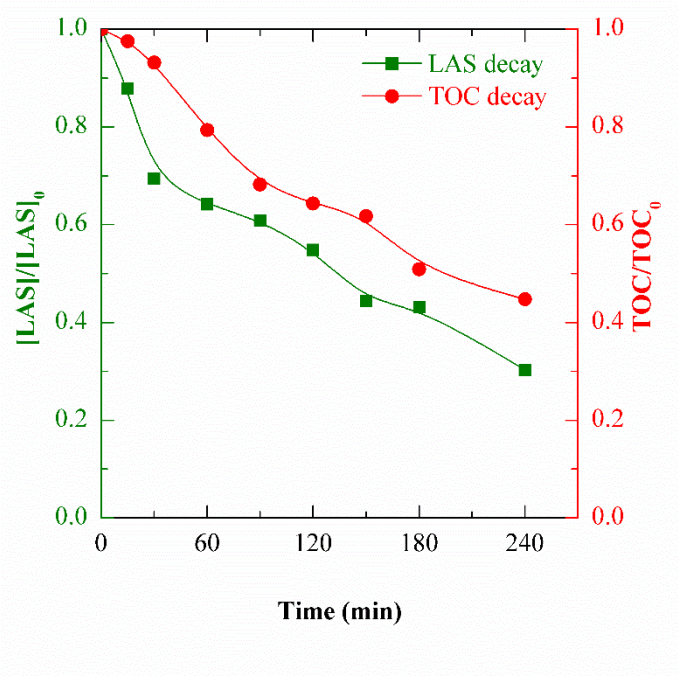
LAS decay
TOC decay
[LAS]/[LAS]0
TOC/TOC0
Time (min)
0
60
120
180
240
0.0
0.2
0.4
0.6
0.8
1.0

Fig. 11

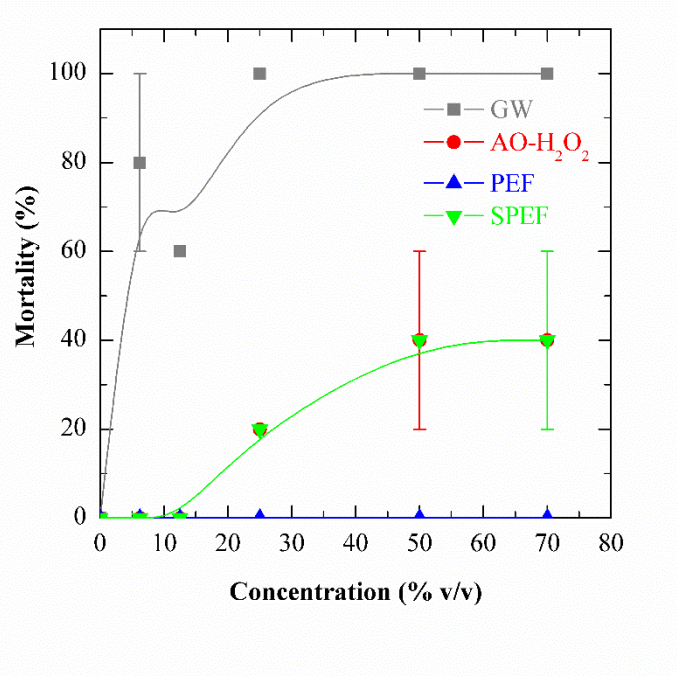
Mortality (%)
Concentration (% v/v)
GW
AO-H2O2
PEF
SPEF
0
20
40
60
80
100
0
10
20
30
40
50
60
70
80

Fig. 12

Table 1.

Literature data collected for different technologies applied to the treatment of GW and GW-like effluents.

Treatment	Effluent type[a]	Main goals[b]	Treated volume or Flowrate	System	Removals	Energy consumption	Reference
Hydroponic green roof	Synthetic GW	Collect, treat and use greywater in green buildings	207 L per batch	Seven carbon steel tanks (400 mm × 400 mm × 300 mm) containing three-year-old plants of *Lonicera Japonica*	81% COD, 97% BOD_5, 88% anionic surfactants, 75% turbidity	-	[40]
Biodegradation	Synthetic WW + LAS	Investigate the efficiency of LAS biodegradation using fungi (*Penicillium chrysogenum*) in a biological system in batch. The effect of concentrations of LAS and ammonium sulfate in the aerobic cultures was evaluated using a 2^2 full factorial design	0.07 L per batch	The synthetic medium was inoculated with spore solution (100 µL per 0.070 L of medium), followed by incubation for 5 days, at 25 °C and 180 rpm	99.5% LAS biodegradation, with low residual dry mass (0.2995 g)	-	[41]
Biofiltration and electrochemical disinfection	Synthetic GW + Urban WW from a secondary treatment	Assess the performance of a disinfection process with BDD anode when an SPE is used to treat GW pre-treated using a green-wall biofilter	1 m^2 day^{-1}	The electrochemical system consisted of a sandwich of two compartments containing a 40-cm^2 Nb|BDD mesh anode, a cation exchange membrane (CEM) and a 40-cm^2 stainless-steel mesh cathode	98.5% COD, 98.6% BOD_5, 95.4% turbidity, 90.4% TOC, 98.4% TSS, 88.9% *E. coli*, 88.3% of total coliforms	0.63–0.83 kWh m^{-3} for > 99.9% removal of *E. coli* and total coliforms	[42]
Anaerobic filter + UV disinfection	GW	Discuss aspects related to GW reuse in airports, as well as to present a case study in Brazil. Evaluate the decay of BOD_5, COD, turbidity, TSS and NO_3^-, as well as the disinfection ability	2.82 m^3 day^{-1}	The anaerobic filter was made of fiberglass and was 1.80 m high with a diameter of 1.00 m (1.41 m^3). It was coupled to the UV disinfection system; the 36-W UV lamps provided a UV radiation intensity of 114 mW cm^{-2}	73% BOD_5, 72% COD, 77% TSS, 88% turbidity, 60% NO_3^-	64 kWh m^{-3}	[43]
Ultrafiltration	WME + SDBS	Evaluate the influence of various experimental parameters on the removal of SDBS (100-1000 mg L^{-1}).	1.0 L per batch	The effluent was pumped from a stirred tank to a filter-press type reactor equipped with ceramic ultrafiltration membranes of 1 and 5 kDa (TiO_2), or 15 to 150 kDa (ZrO_2)	Up to 65% removal of 1000 mg L^{-1} SDBS using 1 kDa ceramic membrane, applying 1.5 bar at room temperature	-	[44]
Filtration + Ozonation	GW	Evaluate the influence of O_3 dosage and contact time on the removal of BOD_5, COD, turbidity, TSS, *E. coli*, total coliforms and pathogenic bacteria	6 m^3 day^{-1}	A pilot system containing a 1.3 m^3 storage tank, connected to sand filtration vessels, followed by filtration vessels containing granular activated carbon of similar capacity, and then a corona discharge O_3 generator. A recirculation system received and kept in contact the effluent obtained from the filters with the generated O_3	Applying 5-20 g h^{-1} O_3 for 2 h at a flowrate of 20 L min^{-1}, a removal of 8.8% turbidity and 2.8% TSS, as well as total disinfection was obtained	10.09 kWh day^{-1} (1.80 kWh m^{-3}).	[45]
Chemical coagulation–flocculation + UV photolysis	Synthetic anionic surfactant WW + LAS	Optimize the operation conditions using factorial design methodologies and response surface analysis	0.2–0.4 L per batch	Coagulation-flocculation was made in a classical jar test apparatus. UV photolysis was carried out using a high pressure Hg lamp (quartz tube, 36 W, λ = 253.7 nm) placed 5 cm above the surface of the solution	71.3% and 74.6% of LAS from the synthetic LAS wastewater and the MWE, respectively	-	[46]

Electrocoagulation	GW	Evaluate the use of various experimental parameters on the removal of COD, TSS, TN, TP, anionic surfactant concentration and turbidity	0.6 L per batch	Undivded electrochemical reactor operated in batch mode, equipped with 4 metal plates (2 anodes and 2 cathodes)	Up to 99% COD removal at 1 mA cm^{-2} and initial pH = 7.6	9.46 kWh m^{-3}	[2]
Electrocoagulation	GW	Reach reuse limits	1.5 L per batch	A perspex glass reactor filled with 1.5 L kept under stirring. Al plates (8.5 cm × 8.5 cm × 2 mm) were used as the anode and cathode. The distance between electrodes was considered as 1 cm	70% COD, 87.5% BOD, 82.7% nitrate, 84.7% phosphate	0.153 kWh m^{-3}	[47]
Membrane filtration + Electrochemical technologies + Adsorption	WME	Evaluate the removal of TSS COD, turbidity and NPEO3-17	1 – 3 L per batch	Tested sequence: (1) Ultrafiltration (UF) of WME; (2) electrocoagulation/electrooxidation (EC/EO) of the concentrate from UF; (3) electrooxidation (EO) of the filtrate from UF; (4) adsorption of UF filtrate; (5) nanofiltration of UF filtrate; and (6) EO of NF concentrate. In EO: BDD, Ti/Pt and Ti/IrO_2 anodes, as well as graphite, glassy carbon and Ti/Pt cathodes	50% COD, 95% TSS, 97% turbidity, 75% NPEO3-17	-	[48]
EAOPs (EF and PEF with and without peroxymonosulfate)	WME	Evaluate the use of various experimental parameters on the removal of COD, TOC and color	0.2 L per batch	Batch-type undivided electrochemical reactor (6 cm × 10 cm) equipped with a grafite-felt cathode (5 cm × 5 cm × 0.5 cm), with air flowrate of 1 L min^{-1}, and Pt sheet anode (2 cm × 3 cm) with interelectrode distance of 2 cm	99.5% COD and 97% TOC after 180 min at 30 mA cm^{-2}, 2 mM PMS, 100 mg L^{-1} MNPs, pH = 5.0,	-	[49]
EAOPs (EF)	WW	Investigate the effect of experimental parameters on the removal of COD and TSS using four factors three levels Box–Behnken response surface design	0.7 L per batch	900 mL glass beaker. Iron plates were used as a anode and cathode (each with 20 cm^2)	90% COD and 85% TSS after 14 min at 10 mA cm^{-2}, H_2O_2/Fe^{2+} = 0.70 and pH = 4	-	[50]
EAOPs (AO-H_2O_2, PEF, SPEF)	GW	Discuss the performance of various EAOPs using a factorial design	0.1–10 L per batch	Bench-scale electrochemical reactor with capacity of 150 mL, equipped with a BDD thin film as the anode and a carbon-PTFE air-diffusion cathode (both of 3 cm^2). Air flowrate of 2 L min^{-1}. SPEF pre-pilot system: filter-press electrochemical cell (electrodes of 20 cm^2) coupled to a CPC solar photoreactor. comprising a 20-L reservoir tank; liquid flowrate of 180 L min^{-1}	LAS and TOC removals after 240 min: 84% and 37% in AO-H_2O_2, 63% and 78% in PEF, 70% and 55% in SPEF	AO-H_2O_2: 0.13 – 23.9 kWh (kg TOC)$^{-1}$ PEF: 0.05 – 6.52 kWh (kg TOC)$^{-1}$ SPEF: 0.32 kWh (kg TOC)$^{-1}$	This work

[a] GW: greywater; SDBS: sodium dodecyl-benzene sulfonate; WME: washing machine effluent; WW: wastewater. [b] BOD_5: biological oxygen demand after 5 days; COD: chemical oxygen demand; NPEO3-17: nonylphenol ethoxylates; TN: total nitrogen; TP; total phosphorus; TSS: total suspended solids.

Table 2.

Raw GW characterization.

Physicochemical parameters	
pH	6.7-7.6
Conductivity (µS cm^{-1})	162.5-390
Turbidity (NTU)	57.8-78.6
COD (mg L^{-1})	283-352
$BOD_{(5,20)}$ (mg L^{-1})	270-280.0
TOC (mg L^{-1}) before LAS addiction	50.3
TOC (mg L^{-1}) after LAS addiction	80.8-100.6
TIC (mg L^{-1})	52.0 – 75.0
Cl^- (mg L^{-1})	20-30
NH_3–N (mg L^{-1})	0.5-3.1
NO_3^- (mg L^{-1})	0.1-2.1
Total nitrogen (mg L^{-1})	0.6-5.2
Total solids (mg L^{-1})	113-451
Dissolved solids (mg L^{-1})	17-68
Fe (mg L^{-1})	<0.05-0.20
PO_4^{3-} (mg L^{-1})	50-68
Al (mg L^{-1})	0.100-3.550
Ba (mg L^{-1})	< 1
Ca (mg L^{-1})	15-17
Zn (mg L^{-1})	0.37-1.60
Mn (mg L^{-1})	0.061
Ni (mg L^{-1})	<0.025
Hg (mg L^{-1})	<0.0003
Cr (mg L^{-1})	<0.05
Cd (mg L^{-1})	<0.006
Pb (mg L^{-1})	<0.063

Table 3.

Observed and predicted values for the percentages of degradation of LAS ($Y_{\%Deg}$) and mineralization ($Y_{\%Min}$), corresponding to the AO-H_2O_2 treatment of 100 mL of GW in 0.050 M Na_2SO_4 using the projected experimental design, and estimated energy consumption per unit TOC (EC_{TOC}).

Experiment	$X_{[LAS]}$ (mg L^{-1})	X_j (mA cm^{-2})	X_t (min)	$Y_{\%Deg}$		$Y_{\%Min}$		EC_{TOC} (kWh (kg TOC)$^{-1}$)
				Observed	**Predicted**	**Observed**	**Predicted**	
1	80	32.5	10	8.58	8.58	12.86	12.86	0.13
2	40	32.5	120	76.09	76.09	29.11	29.11	0.89
3	40	77.5	10	5.56	5.56	0.54	0.54	23.9
4	40	77.5	120	70.09	70.09	28.54	28.54	5.43
5	60	55	65	45.02	44.56	17.23	17.4	2.36
6	80	32.5	120	68.62	68.62	52.40	52.4	0.37
7	40	32.5	10	7.34	7.34	10.39	10.39	0.21
8	80	77.5	10	21.11	21.11	1.69	1.69	5.73
9	80	77.5	120	83.59	83.59	37.18	37.18	3.13
10	60	55	65	45.21	44.56	16.96	17.4	2.40
11	60	55	65	43.45	44.56	18.01	17.4	2.26

Table 4.

ANOVA table results for factorial design 2^k obtained for GW treatment by AO-H_2O_2 process.

			$Y_{\%Deg}$		
Factor	**SS**	**df**	**MS**	**F-value**	**p-value**
Curvatr.	8.1903	1	8.1903	8.7775	0.09754
(1) $X_{[LAS]}$	65.094	1	65.094	69.761	0.01403
(2) X_j	48.610	1	48.610	52.095	0.01866
(3) X_t	8179.2	1	8179.2	8765.6	0.00011
1 by 2	155.58	1	155.58	166.74	0.00594
1 by 3	14.472	1	14.472	15.510	0.05884
2 by 3	0.39605	1	0.39605	0.42444	0.58159
1*2*3	5.5444	1	5.5444	5.9420	0.13503
Error	1.8662	2	0.93310		
Total SS	8478.9	10			
			$Y_{\%Min}$		
Factor	**SS**	**df**	**MS**	**F-value**	**p-value**
Curvatr.	38.281	1	38.281	128.76	0.00768
(1) $X_{[LAS]}$	157.97	1	157.97	531.37	0.00188
(2) X_j	169.37	1	169.37	569.70	0.00175
(3) X_t	1852.9	1	1852.9	6232.4	0.00016
1 by 2	31.880	1	31.880	107.23	0.00920
1 by 3	100.18	1	100.18	336.97	0.00295
2 by 3	3.4191	1	3.419	11.500	0.07704
1*2*3	22.211	1	22.211	74.710	0.01312
Error	0.59460	2	0.29730		
Total SS	2376.8	10			

SS: Sum-of-Square; df: degree of freedom; MS: Mean Square.

Table 5.

Estimated effect, regression coefficients and corresponding "t" and "p" values of influent factors in $Y_{\%Deg}$ and $Y_{\%Min}$ responses forGW treatment by AO-H_2O_2.

$Y_{\%Deg}$						
Factor	**Effect**	**Standard Error Effect**	**t-value**	**p-value**	**Coefficient**	**Standard Error Coefficient**
Mean/Interac.	42.622	0.34152	124.801	0.00006	42.622	0.34152
Curvatr.	3.8750	1.3079	2.9627	0.09754	1.9375	0.65396
(1) $X_{[LAS]}$	5.7050	0.68304	8.3523	0.01403	2.8525	0.34152
(2) X_j	4.9300	0.68304	7.2177	0.01866	2.4650	0.34152
(3) X_t	63.950	0.68304	93.625	0.00011	31.975	0.34152
1 by 2	8.8200	0.68304	12.913	0.00594	4.4100	0.34152
1 by 3	-2.6900	0.68304	-3.9382	0.05884	-1.3450	0.34152
2 by 3	-0.44500	0.68304	-0.65150	0.58159	-0.22250	0.34152
1*2*3	1.6650	0.68304	2.4376	0.13503	0.83250	0.34152
$Y_{\%Min}$						
Factor	**Effect**	**Standard Error Effect**	**t-value**	**p-value**	**Coefficient**	**Standard Error Coefficient**
Mean/Interac.	21.589	0.19277	111.99	0.00008	21.589	0.19277
Curvatr.	-8.3775	0.73827	-11.347	0.00768	-4.1890	0.36914
(1) $X_{[LAS]}$	8.8875	0.38555	23.051	0.00188	4.4437	0.19278
(2) X_j	-9.2025	0.38555	-23.868	0.00175	-4.6012	0.19278
(3) X_t	30.437	0.38555	78.945	0.00016	15.219	0.19278
1 by 2	-3.9925	0.38555	-10.355	0.00920	-1.9962	0.19278
1 by 3	7.0775	0.38555	18.357	0.00295	3.5387	0.19278
2 by 3	1.3075	0.38555	3.3912	0.07704	0.65375	0.19278
1*2*3	-3.3325	0.38555	-8.6435	0.01312	-1.6662	0.19278

Table 6.

Observed and predicted values for the percentages of degradation of LAS ($Y_{\%Deg}$) and mineralization ($Y_{\%Min}$), corresponding to the PEF treatment of 100 mL of GW in 0.050 M Na_2SO_4 using the projected experimental design, and estimated energy consumption per unit TOC (EC_{TOC}).

Experiment	$X_{[Fe^{2+}]}$ (mg L^{-1})	X_j (mA cm^{-2})	X_t (min)	$Y_{\%Deg}$		$Y_{\%Min}$		EC_{TOC} (kWh (kg TOC)$^{-1}$)
				Observed	Predicted	Observed	Predicted	
1	5	77.5	120	63.12	62.62	78.28	78.04	1.86
2	25	32.5	120	62.50	61.99	66.50	66.26	0.37
3	5	77.5	10	16.90	17.40	45.69	45.93	0.27
4	5	32.5	10	14.91	14.41	33.88	33.64	0.06
5	5	32.5	120	58.90	59.40	73.18	73.42	0.33
6	15	55	65	41.60	41.76	53.05	47.12	0.84
7	25	77.5	10	10.20	9.70	5.61	5.39	2.16
8	15	55	65	38.40	41.76	42.96	47.12	1.04
9	25	32.5	10	21.40	21.90	41.19	41.43	0.05
10	25	77.5	120	49.51	50.01	22.28	22.52	6.52
11	15	55	65	45.29	41.76	45.35	47.12	0.99

Table 7.

ANOVA table for factorial design 2^k obtained for GW treatment by PEF process.

$Y_{\%Deg}$					
Factor	**SS**	**df**	**MS**	**F-value**	**p-value**
Curvatr.	45.833	1	45.833	5.3302	0.10415
(1) $X_{[Fe2+]}$	13.056	1	13.056	1.5184	0.30563
(2) X_j	40.410	1	40.410	4.6995	0.11870
(3) X_t	3638.9	1	3638.9	423.19	0.00025
1 by 2	115.52	1	115.52	13.434	0.03511
1 by 3	12.005	1	12.005	1.3961	0.32250
2 by 3	0.02420	1	0.02420	0.00281	0.96103
Error	25.796	3	8.5987		
Total SS	3891.5	10			
$Y_{\%Min}$					
Factor	**SS**	**df**	**MS**	**F-value**	**p-value**
(1) $X_{[Fe2+]}$	1138.8	1	1138.8	76.277	0.00095
(2) X_j	494.39	1	494.39	33.114	0.00452
(3) X_t	1620.8	1	1620.8	108.56	0.00048
1 by 2	1169.1	1	1169.1	78.304	0.00090
1 by 3	111.82	1	111.82	7.4899	0.05208
2 by 3	29.453	1	29.453	1.9727	0.23285
Error	59.721	4	14.930		
Total SS	4624.1	10			

SS: Sum-of-Square; df: degree of freedom; MS: Mean Square

Table 8.

Effect Estimates, regression coefficients and corresponding "t" and "p" values of influent factors in $Y_{\%Deg}$ and $Y_{\%Min}$ responses for GW treatment by PEF.

$Y_{\%Deg}$						
Factor	**Effect**	**Standard Error Effect**	**t-value**	**p-value**	**Coefficient**	**Standard Error Coefficient**
Mean/Interac.	37.180	1.0367	35.862	0.00005	37.180	1.0367
Curvatr.	9.1667	3.9704	2.3087	0.10415	4.5833	1.9852
(1) $X_{[Fe2+]}$	-2.5550	2.0735	-1.2322	0.30563	-1.2775	1.0367
(2) X_j	-4.4950	2.0735	-2.1678	0.11870	-2.2475	1.0367
(3) X_t	42.655	2.0735	20.572	0.00025	21.327	1.0367
1 by 2	-7.6000	2.0735	-3.6653	0.03511	-3.8000	1.0367
1 by 3	-2.4500	2.0735	-1.1816	0.32250	-1.2250	1.0367
2 by 3	0.11000	2.0735	0.05305	0.96103	0.05500	1.0367
$Y_{\%Min}$						
Factor	**Effect**	**Standard Error Effect**	**t-value**	**p-value**	**Coefficient**	**Standard Error Coefficient**
Mean/Interac.	46.179	1.1650	39.638	0.000002	46.179	1.1650
(1) $X_{[Fe2+]}$	-23.862	2.7322	-8.7337	0.00095	-11.931	1.3661
(2) X_j	-15.722	2.7322	-5.7544	0.00452	-7.8612	1.3661
(3) X_t	28.467	2.7322	10.419	0.00048	14.234	1.3661
1 by 2	-24.177	2.7322	-8.8490	0.00090	-12.089	1.3661
1 by 3	-7.4775	2.7322	-2.7368	0.05208	-3.7387	1.3661
2 by 3	-3.8375	2.7322	-1.4045	0.23285	-1.9187	1.3661